Progress in Materials Science 54 (2009) 1059–1100

Contents lists available at ScienceDirect

Progress in Materials Science

journal homepage: www.elsevier.com/locate/pmatsci

Merger of structure and material in nacre and bone – Perspectives on *de novo* biomimetic materials

Horacio D. Espinosa [a,*], Jee E. Rim [a], Francois Barthelat [a,1], Markus J. Buehler [b]

[a] *Mechanical Engineering, Northwestern University, Evanston, IL 60208, USA*
[b] *Department of Civil and Environmental Engineering, Massachusetts Institute of Technology, 77 Massachusetts Ave., Room 1-235A&B, Cambridge, MA 02139, USA*

ARTICLE INFO

Article history:
Received 19 March 2009
Received in revised form 1 April 2009
Accepted 22 May 2009

ABSTRACT

In contrast to synthetic materials, evolutionary developments in biology have resulted in materials with remarkable structural properties, made out of relatively weak constituents, arranged in complex hierarchical patterns. For instance, nacre from seashells is primarily made of a fragile ceramic, yet it exhibits superior levels of strength and toughness. Structural features leading to this performance consist of a microstructure organized in a hierarchical fashion, and the addition of a small volume fraction of biopolymers. A key to this mechanical performance is the cohesion and sliding of *wavy* ceramic tablets. Another example is bone, a structural biological material made of a collagen protein phase and nanoscopic mineral platelets, reaching high levels of toughness and strength per weight. The design and fabrication of *de novo* synthetic materials that aim to utilize the deformation and hardening mechanism of biological materials such as bone or nacre is an active area of research in mechanics of materials. In this review, our current knowledge on microstructure and mechanics of nacre and bone are described, and a review of the fabrication of nacre-inspired artificial and related materials is presented. Both experimental and simulation approaches are discussed, along with specific examples that illustrate the various approaches. We conclude with a broader discussion of the interplay of size effects and hierarchies in defining mechanical properties of biological materials.

* Corresponding author.
E-mail address: espinosa@northwestern.edu (H.D. Espinosa).
[1] Present address: Mechanical Engineering, McGill University, 817 Sherbrooke Street West, Montreal, Quebec, Canada H3A 2K6.

0079-6425/$ - see front matter © 2009 Elsevier Ltd. All rights reserved.
doi:10.1016/j.pmatsci.2009.05.001

Contents

1. Introduction

Natural and biological materials can exhibit remarkable combinations of stiffness, low weight, strength and toughness, which are in some cases unmatched by synthetic materials. In the past two decades significant efforts were undertaken, by the materials research community, to elucidate the microstructure and mechanisms that enable these mechanical performances. These efforts were facilitated by the advancement of experimental and theoretical tools to assess the relation between structure and properties. Novel concepts for the design of artificial materials mimicking them were also advanced [1–5].

The mechanical performance of synthetic and natural materials is illustrated in Fig. 1. Fig. 1a depicts toughness versus Young's modulus of synthetic materials such as metals, alloys and ceramics. Fig. 1b is a material properties map for a selection of natural ceramics, biopolymer and their composites [6]. The upper left corner of the map shows relatively soft pure protein materials such as skin, with a mechanical behavior similar to elastomers. The lower right corner of the chart shows stiff but brittle minerals such as hydroxyapatite or calcite. Most hard biological materials incorporate minerals into soft matrices, mostly to achieve the stiffness required for structural support or armored protection [7]. These materials are seen in the upper right part of the map and show how natural materials achieve high stiffness by incorporating minerals while retaining an exceptional toughness. Alternatively, one can consider how natural materials turn brittle minerals into much tougher materials, in some cases only with a few percent addition of biopolymers. These materials have in general relatively complex structures organized over several length scales (hierarchical structures [1,2]) leading to mechanisms that operate over several length scales, down to the nanoscale [8–10]. These hierarchical, multi-scale structures are found in abundance virtually all throughout biology, where they form a diverse range of materials that include bone, tendon (based on collagen), cells or skin. In some cases, organisms are formed out of mineralized structures, such as the deep sea sponge *Euplectella* sp. [11].

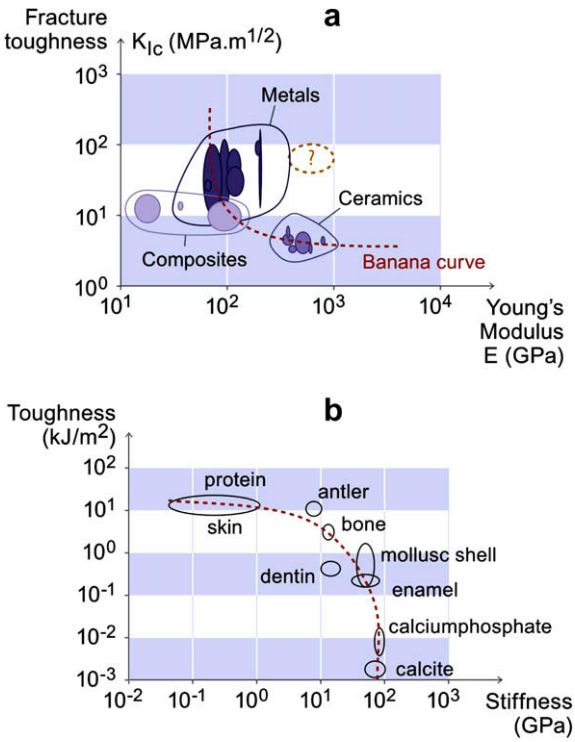

Fig. 1. Performance of engineered and biological materials in the stiffness–toughness domain. Subplot (a) depicts toughness and stiffness values for synthetic materials, such as metals, alloys and ceramics (plot adapted from Ashby et al. [120]). Subplot (b) compares the toughness and stiffness properties for a number of biological materials (plot adapted from Fratzl et al. [121]). Biological composites, such as antler, dentin, bone and enamel are result of a "reinforcing" combination of the protein toughness and the mineral-stiffness. Remarkably, all these materials lie – in contrast to biological materials – on a so-called "banana-curve", an inverse relation between increasing toughness an decreasing stiffness. The yellow region shows the property region of high toughness and stiffness that may be accessible through designing bio-inspired materials (For interpretation of the references to colour in this figure legend, the reader is referred to the web version of this article.).

Mollusc shells are an excellent example of such high-performance natural materials. Mollusks are composed of at least 95% of minerals such as calcium carbonate (calcite, aragonite), a brittle material, yet they exhibit a toughness ≈3000 times higher than calcite (see Fig. 1b), at the expense of a small reduction in stiffness. How is such performance achieved? Can it be duplicated in artificial materials? This review provides first an overview of the evolution of materials in Molluscs and other organisms, along with their general characteristics. Then we focus on the detailed structure and mechanics of nacre from Red Abalone, and include a discussion of other mineralized tissues and organisms (e.g., bone). The comparison of bone's structure with nacre provides the basis for a discussion of universal features found across a broader range of biological materials; suggesting particularly successful material concepts utilized to provide appropriate biological functionality. Computational approaches, complementing experimental studies, will be reviewed and discussed in the context of case studies of the analysis of deformation of nacre, bone and protein-based hierarchical protein filaments, elucidating mechanisms of how biological materials can combine high strength at high levels of robustness against catastrophic failure. Synthetic materials, inspired by the intricate structure and mechanisms of nacre and bone, are discussed together with future trends in biomimetic materials design approaches including materials that mimic the structure of biological materials.

1.1. Mollusc shells: overview

Molluscs appeared 545 million years ago, and comprise about 60,000 species [12]. They have a very soft body (*mollis* means soft in Latin) and most of them grow a hard shell for protection. The earlier molluscs were small (2–5 mm) with shell structures very similar to the modern forms. The size and the diversity of the mollusc family increased dramatically 440–500 million years ago, with the apparition of various classes. Currently the class which includes the largest number of species is the *Gastropoda*, with about 35,000 living species. These include mostly marine species (Conch shell, top shell, abalone), but also land species (land snails). The second largest class, the *Bivalvia*, counts about 10,000 species and includes clams, oysters and freshwater mussels.

The shell of molluscs is grown by the mantle, a soft tissue that covers the inside of the shell [13]. A great variety of shell structures has emerged from this process. They include prismatic, foliated and cross lamellar structure, columnar and sheet nacre (Fig. 2). All of these structures use either calcite or aragonite, with a small amount of organic material which never exceeds 5% of the composition in weight. In order to provide an efficient protection, the shell must be both stiff and strong. Mechanical tests on $\approx$20 distinct species of seashells by Currey and Taylor [14] revealed an elastic modulus ranging from 40 GPa to 70 GPa, and a strength in the range of 20–120 MPa. By comparison, human femoral bone is softer (E = 20 GPa) but stronger (150–200 MPa strength). Amongst all the structures found in shells, nacreous structures appear to be the strongest: The strength of nacre can reach 120 MPa for the shell Turbo, as opposed to a maximum of 60 MPa for other non-nacreous structures. The superior strength of nacre has been reconfirmed in several other recent studies [15–19].

The shells of molluscs offer a perfect example of a lightweight, tough armor system, that now serve as models for *de novo* armor designs. The structure and mechanical properties of the materials that compose these shells are of particular interest, and they are the focus of numerous studies.

1.2. Multi-scale experimental and simulation analysis of biological materials

The analysis of material properties at multiple scales is a crucial issue in understanding biological materials, as their structure changes with hierarchical level (and thus length-scale), and therefore most material properties are strongly dependent on the scale of observation. Multi-scale experimental and simulation analyses are the key to improve our systematic understanding of how structure and properties are linked.

Experimental techniques have gained unparalleled accuracy in both length- and time-scales (see Fig. 3), as reflected in development and utilization of Atomic Force Microscope (AFM) [20,21], magnetic and optical tweezers [22,23] or nanoindentation [24] to analyze biological materials [25]. Additional approaches based on MEMS testing of materials at micrometer length-scales provide exciting opportunities to bridge the gap between the molecular nanoscale and macroscopic scales [26–29].

Modeling and simulation have evolved into predictive tools that complement experimental analyses at comparable length- and time-scales. The use of bottom-up atomistic models based on the chemical structure of materials has been a very fruitful approach in describing the behavior of complex biological and natural materials, at length- and time-scales overlapping with experimental methods. Fig. 3 shows how simulation and experimental approaches can be integrated to assess material properties across multiple time- and length-scales. In the following sections, we provide a brief review of some widely used simulation methods.

1.2.1. Molecular dynamics

Atomistic molecular dynamics (MD) is a suitable tool for elucidating the atomistic mechanisms that control deformation and rupture of chemical bonds at nano-scale, and to relate this information to macroscopic materials failure phenomena (see, e.g., review articles and books [30–32]). The basic concept behind atomistic simulation via MD is to calculate the dynamical trajectory of each atom in the material, by considering their atomic interaction potentials, by solving each atom's equation of motion according to $F = ma$, leading to positions $r_i(t)$, velocities $v_i(t)$ and accelerations $a_i(t)$.

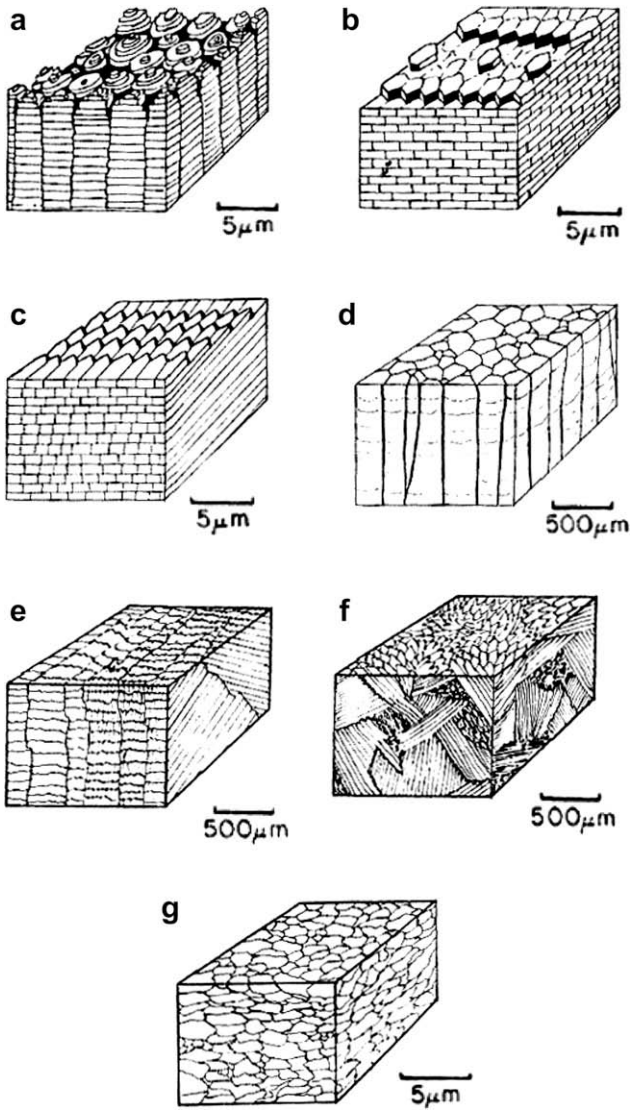

Fig. 2. Mineral structures found in seashells: (a) columnar nacre; (b) sheet nacre; (c) foliated; (d) prismatic; (e) cross-lamellar; (f) complex crossed-lamellar; (g) homogeneous. Reproduced with permission from [14].

1.2.2. Multi-scale approaches

The integration of multiple simulation methods of different levels of accuracy into the description of materials is referred to as multi-scale simulations. At smaller-scales, more accurate simulation methods are used to feed parameters into methods that provide a coarse, computationally less expensive description of materials. The seamless link between different methods (Fig. 3) provides a means to bridge the scales from atoms (the level of chemistry) to the continuum.

The use of such methods is motivated by the fact that albeit being a very accurate description of macromolecules, all-atom modeling approaches have historically been prohibitively extensive when

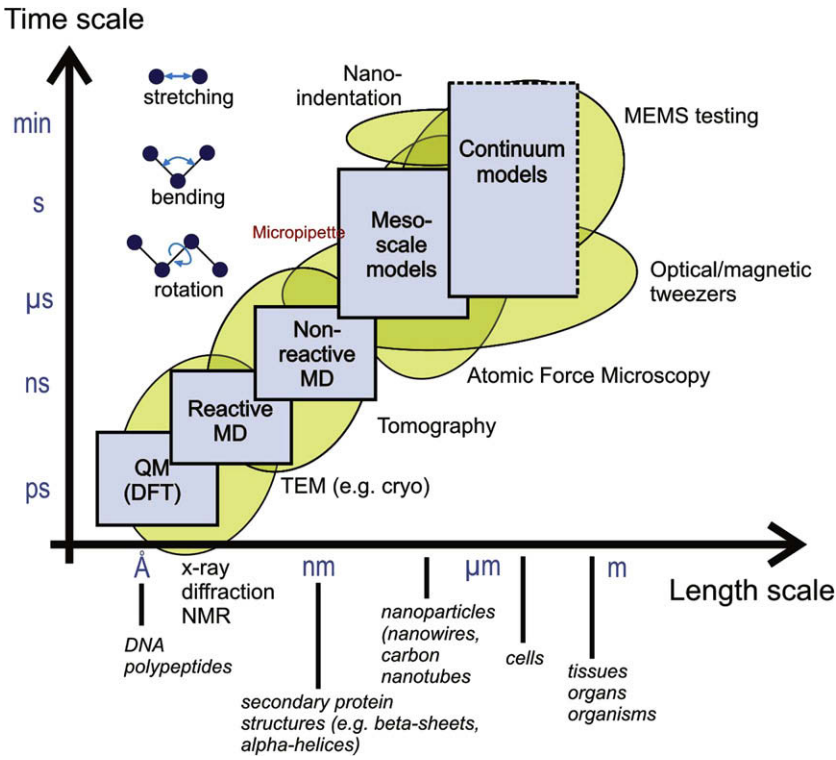

Fig. 3. Integration of multi-scale experimental and simulation approaches in the analysis of biological materials. The inlay depicts the formulation of the molecular dynamics approach, by describing the individual energy contributions of bond stretching, bending, rotation, etc [32].

large systems and long simulation times must be considered. This lead to the development of coarse-grained models [33], which provide simplified representations of macromolecules employing less degrees of freedom and simple bonded and non-bonded interactions that can be rapidly calculated in each time step. Coarse-grained models have so far been successfully applied to a wide range of problems including protein folding, allostery, aggregation, molecular biomechanics as well as multi-scale description of complex materials such as bone. The various approaches are briefly reviewed here.

Single bead models are perhaps the earliest approach taken for studying macromolecules. The term single-bead derives from the idea of using single beads (masses) for describing each amino acid in a protein structure. The Elastic Network Model (ENM) [34], the Gaussian Network Model (GNM) [35] and the Go-model [36] are well known examples of this simplified approach. Using more than one bead per amino acid can lead to a more detailed description of macromolecules. In the simplest case, the addition of another bead can be used to describe specific side-chain interactions [37]. Four to six bead models capture an even higher amount of detail by explicit or united atom description for backbone carbon atoms, side chains, carboxyl and amino groups of amino acids. A great example of this approach is the coarse-grained models developed in Hall's group for studying folding and aggregation in proteins using discontinuous molecular dynamics [38,39]. More recently, coarser-level modeling approaches have been applied to model biomolecular systems at larger time- and length-scales. These models typically employ superatom descriptions that treat clusters of amino acids as "beads", as shown schematically in Fig. 4 for the case of tropocollagen molecules, the basic building block of bone. In such models, the elasticity of the polypeptide chain is captured by simple harmonic or anharmonic (nonlinear) bond and angle terms. Such methods are computationally quite efficient and capture for example shape dependent mechanical phenomena in large biomolecular structures [40], and

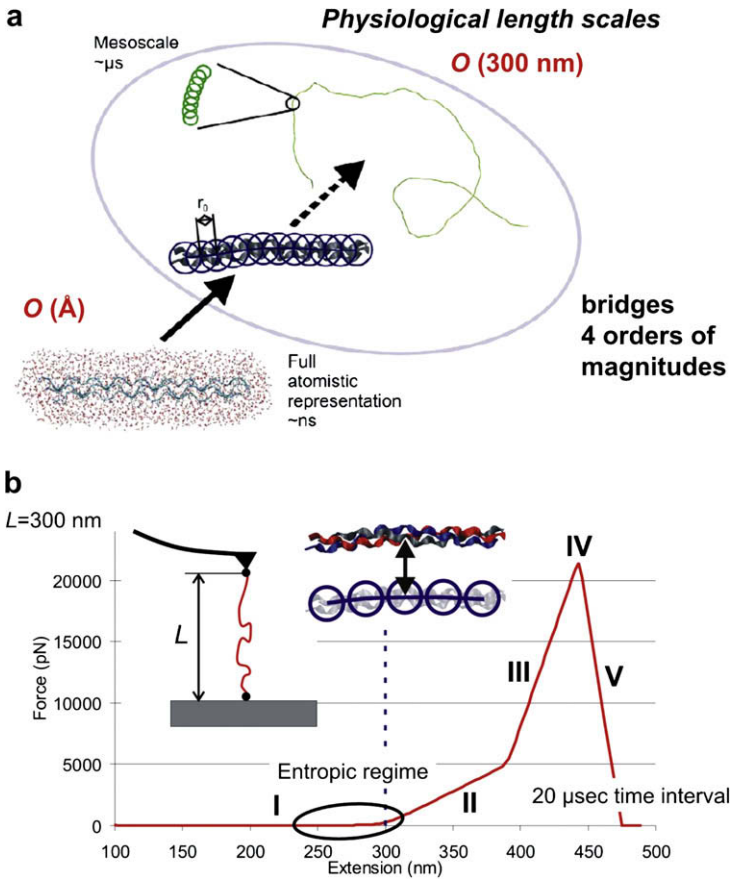

Fig. 4. (a) Illustration of the coarse-graining approach for a simple one-dimensional fibrillar protein filament (single tropocollagen molecule). This schematic illustrates how a full atomistic representation is coarse-grained and used in a mesoscale model formulation. The mesoscale model formulation enables one to reach much larger time- and length-scales. The systematic parameterization from the bottom up provides a rigorous link between the chemical structure of proteins (for example, through their amino acid sequence) and the overall functional material properties. This computational approach is a key component, as it provides us with the ability to reach microsecond- and micrometer length-scales. (b) Application of this approach in elucidating the force-extension behavior of a 300 nm long tropocollagen molecule [83].

can also be applied to collagen fibrils in connective tissue [41] as well as mineralized composites such as bone [42]. A case study based on this method applied to bone will be presented in this review article.

2. Nacre

Nacre from seashell is an example showing how evolution can lead to a high performance material made out of relatively weak constituents. Nacre can be found inside many species of seashells from the gastropods and bivalves groups (Fig. 5). Nacre is mostly made of a mineral (aragonite $CaCO_3$, 95% vol.), arranged together with a small amount (5% vol.) of softer organic biopolymers [1]. While mostly made of aragonite, nacre is 3000 tougher than aragonite [6]. The structures and mechanisms behind this remarkable performance are examined in this section.

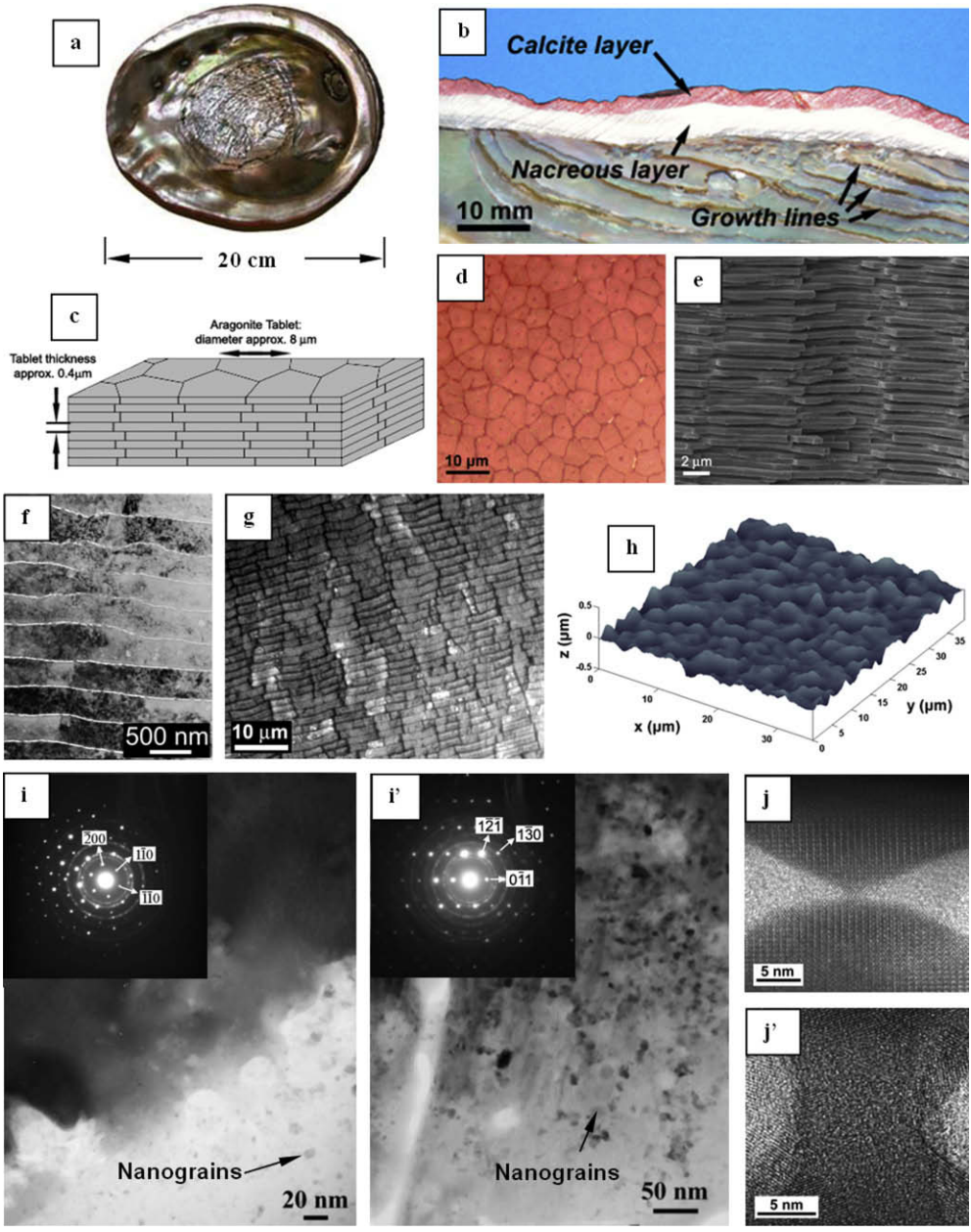

Fig. 5. The multiscale structure of nacre (all images from red abalone except g): (a) inside view of the shell; (b) cross section of a red abalone shell; (c) schematic of the brick wall like microstructure; (d) optical micrograph showing the tiling of the tablets; (e) SEM of a fracture surface; (f) TEM showing tablet waviness (red abalone); (g) optical micrograph of nacre from fresh water mussel (*L. cardium*); (h) topology of the tablet surface from laser profilometry; (i, i′) TEM images showing single aragonite crystal with some nanograins (rings on the SAD); (j, j′) HRTEM of aragonite asperity and bridge (For interpretation of the references to colour in this figure legend, the reader is referred to the web version of this article.).

2.1. Overview of nacre

Numerous mechanical experiments and models were therefore used to pinpoint which microstructural features are behind this performance, in the quest to duplicate them in artificial materials. It is now widely recognized that tablet sliding is a key mechanism in the toughness of nacre [16–19,43]. Because this mechanism is controlled by the interface between the tablets, many efforts have focused on investigating nanoscale mechanisms between the tablets [17,44–47]. More recently, it was shown that these nanoscale mechanisms, while necessary, are not sufficient to explain the behavior of nacre at the macroscale [19,43]. Another key mechanism is actually found at the microscale, where the waviness of tablets generates progressive locking, hardening and spreading of non-linear deformation around cracks and defects. The associated viscoplastic energy dissipation at the interfaces between tablets greatly enhances the toughness of nacre, arresting cracks before they become a serious threat to the shell and to the life of the animal. Nacre is therefore a perfect example of a natural material, which developed a highly sophisticated microstructure for optimal performance, over millions of years of evolution. The structure and mechanisms of this remarkable material are now inspiring the design of the next generation of synthetic composites material.

This example illustrates how the occurrence of hierarchies provides the mechanistic basis for energy dissipation mechanisms at multiple scales. This does not only increase the macroscopic fracture toughness but also provides an increased robustness against catastrophic materials failure, as multiple possible mechanisms can be activated even when one or more of them fail to perform the desired function.

2.2. Integration of structure and material

In biology, structural design and materials engineering is unified through formation of hierarchical features with atomic resolution, from nano to macro. As many other biological materials, nacre has a hierarchical structure, meaning that specific structural features can be found at distinct length scales. At the millimeter scale the shell consists of a two-layer armor system, with a hard outer layer (large calcite crystals) and a softer but more ductile inner layer (nacre, Figs. 5a and b). Under external mechanical aggressions the hard calcite layer is difficult to penetrate, but is prone to brittle failure. Nacre, on the other hand, is relatively ductile and can maintain the integrity of the shell even if the outer layer is cracked, which is critical to protect the soft tissues of the animal. This design of hard ceramic used in conjunction with a softer backing plate is believed to be an optimal armor system [1]. Furthermore, within the nacreous layer itself there are a few sub-layers of weaker material, the so called growth lines [48] which may act as crack deflectors [49].

The microscale architecture of nacre resembles a three dimensional brick and mortar wall, where the bricks are densely packed layers of microscopic aragonite polygonal tablets (about 5–8 μm in diameter for a thickness of about 0.5 μm) held together by 20–30 nm thick layers of organic materials (Fig. 5c–e). The tablets in nacre from abalone shell and other gastropods are arranged in columns (*columnar nacre*), while the tablets in nacre from bivalve such as mussels or oyster are arranged in a more random fashion (*sheet nacre*). Remarkably, the arrangement and size of the tablets in nacre is highly uniform throughout the nacreous layer. Optical microscopy on a cleaved nacre surface reveals Voronoi-like contours (Fig. 5d), with no particular orientation within the plane of the layer [19,43,50].

While the tablets are generally described and modeled as flat at the microscale [18,44], they actually exhibit a significant waviness [19,43]. This feature could be observed using optical microscopy, scanning probe microscopy, scanning and transmission electron microscopy. Tablet waviness is not unique to nacre from red abalone (Fig. 5f); it was also observed on another gastropod species (top shell *Trochus niloticus*, Fig. 5h), and in a bivalve (freshwater mussel *Lampsilis Cardium*, Fig. 5g). The waviness of the tablets can be also observed for many other species in the existing literature [1,51–55]. For the case of red abalone, laser profilometry was used to measure a roughness (RMS) of 85 nm, for an average peak-to-peak distance of 3 μm [19,43]. The roughness can reach amplitudes of 200 nm, which is a significant fraction of the tablet thickness (450 nm, Fig. 5f–h) [19,43]. The waviness of the tablets is highly conformal so that the tablets of adjacent layers fit perfectly together.

Nacre exhibits structural features down to the nanoscale. While transmission electron microscopy suggest that the tablets are made of large aragonite grains with a few inclusions of nanograins (Fig. 5i and i′) [1,10], recent scanning probe microscopy observations suggests, indirectly, that the tablet are nanostructured, with grains in the 30 nm range [56,57]. These nanograins have all the same texture and they are delimited by a fine network of organic material [57]. At the 20-30 nm interfaces between the tablets, nanoscale features can also be found. The organic material that fills this space and bonds the tablets together is actually composed of several layers of various proteins and chitin [45,58]. These sheets of organic layers contain pores with a 20–100 nm spacing, leaving space for two types of aragonite structures: nanoasperities (Fig. 5j) and direct aragonite connections across the interfaces (mineral "bridges" connecting tablets, Fig. 5j′). These nanoscale features were observed using scanning probe microscopy [10,55], scanning electron microscopy [13,17] and transmission electron microscopy [10,13,46]. The height and width of these features varies from 10 to 30 nm while their spacing is in the order of 100–200 nm [10]. The density, size and shape of these asperities can vary significantly from one area to another (Fig. 6).

2.3. Deformation of nacre

The deformation behavior of nacre has been studied experimentally using a variety of configurations including uniaxial tension [19,43,59,60], uniaxial compression [10,61], three and four point bending [16,17] and simple shear [19,43]. The behavior of nacre at high strain rates was also explored [61]. Most of these tests were performed on millimeter size specimens. Smaller scales experiments were also used to determine the mechanical response of the individual components of nacre, including nanoindentation on single nacre tablets [10,55,62], and load–extension curves on single molecules of organic materials [45]. At the macroscale, the most striking mode of deformation is in uniaxial tension along the directions of the tablets (it is also the most relevant mode of deformation for nacre within

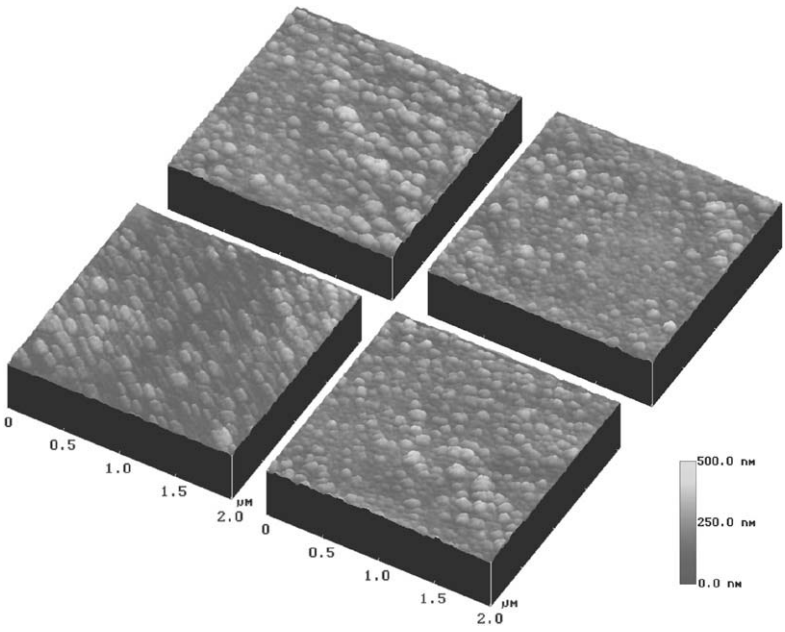

Fig. 6. 2 μm × 2 μm AFM scans from different areas of a cleaved specimen of nacre, showing the surface of the tablets. Asperities of various densities, heights and shapes could be observed. Reproduced with permission from [10].

the shell). Fig. 7a shows the tensile behavior of nacre, showing some ductility at the macroscale (Fig. 7a and b). The stress–strain curve shows relatively large deformations, accompanied by hardening up to failure at a microscopic strain of almost 2%. Full strain field measurement revealed local strain values well in excess of 2% [60]. The transition from elastic to inelastic behavior is progressive (rounding of the curve), which probably results from the statistics of the microstructure. Unloading paths show a decrease in modulus, which indicates progressive accumulation of damage. The tensile behavior of aragonite is also shown in Fig. 7a: linear elastic deformation followed by sudden, brittle failure at small strains. Nacre, although made of 95% of that mineral, exhibit a ductile-like behavior with *relatively* large failure strains.

This remarkable behavior is achieved by the following microscopic mechanism: at a tensile stress of about 60 MPa the interfaces start to yield in shear and the tablets slide on one another, generating local deformation. This phenomenon spreads over large volumes throughout the specimen, which translates into relatively large strains at the macroscale. Once the potential sliding sites are exhausted, the specimen fails by pullout of the tablets (see fracture surface, Fig. 5e), which occurs after local sliding distances of 100–200 nm. This type of micromechanism is unique to nacre, and it is the main source of its superior mechanical properties. For this reason numerous models were developed to capture this behavior [16,18,19,43,63].

In order to achieve such behavior, however, some requirements must be met. First, the interface must be weaker than the tablets; otherwise, the tablets would fail in tension before any significant sliding could occur, which would lead to a brittle type of failure. Strong tablets are important in this regard, and it was shown that their small size confer them with increased tensile strength compared to bulk aragonite [8,59]. It has also been suggested that the presence of nanograins provides some ductility to the tablets [64]. This would increase the tensile strength of the tablets, but would not significantly affect the deformation mode of nacre, which is dominated by tablet sliding. In addition, the

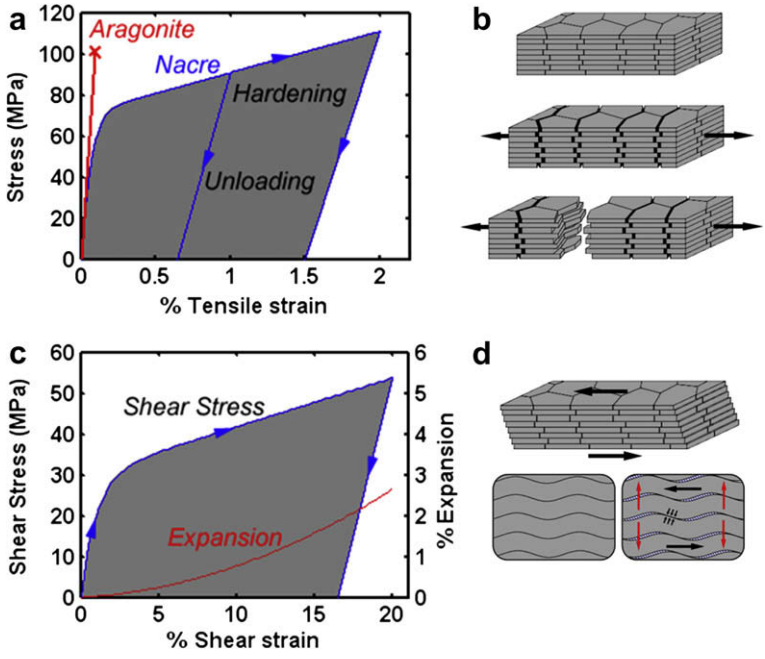

Fig. 7. (a) Experimental tensile stress–strain curve for nacre and (b) associated deformation modes. (c) Experimental shear stress–strain curve for nacre and (d) deformation mechanism. Tablet waviness generates resistance to sliding, accompanied by lateral expansion (red arrows) (For interpretation of the references to colour in this figure legend, the reader is referred to the web version of this article.).

aspect ratio of the tablets must be high enough to maximize sliding areas and produce strong cohesion within the material [65]. However, the aspect ratio is bounded by the fact that too thin tablets would lead to premature tablet failure and brittle behavior. Another fundamental requirement is that some hardening mechanism must take place at the tablet level (meso scale) in order to spread sliding throughout the material. As tablets start to slide, higher stresses are required to slide them further so that it is more favorable for the material to initiate new sliding sites, thus spreading deformation over large volumes. Since the tablets remain essentially elastic in this process, the hardening mechanism has to take place at the interfaces. The best approach to interrogate the behavior of the interface directly is a simple shear test along the layers [19,43]. Shear stress–strain curves reveal a very strong hardening and failure at shear strains in excess of 15% (Fig. 7c). The full strain field, measured by image correlation technique, also captures a significant expansion across the layers [19]. This important observation suggested that the tablets have to climb obstacles in order to slide on one another. Either in tension or shear, strain hardening is the key to large deformation and is essential to the mechanical performance of nacre.

From this observation it is clear that the performance of nacre is controlled by mechanisms at the interfaces between these tablets. In particular, it is important to identify which mechanisms generate resistance to shearing and hardening. Several proposed nanoscale mechanisms (Fig. 8) are discussed next.

First, the tough organic material at the interfaces (Fig. 8a) has an extremely strong adhesion to the tablets [16,45]. Some of the molecules it contains include modules that can unfold sequentially under tensile load, enabling large extensions [45] and maintaining cohesion between tablets over long sliding distances. The load–extension curve of a single protein shows a saw tooth pattern, where each drop in load corresponds to the sequential unfolding of the molecule [45]. When a bundle of these molecules is considered, however, the unfolding processes would operate more or less at constant load. Only when all the modules have unfolded does the chain stiffen significantly (at least upon a 100 nm extension [45]). If this type of molecule is attached to adjacent tablets to ensure their cohesion, little hardening should be expected from them, at least in the first 100 nm or so of tensile or shear deformation of the interface. This type of extension is on the order of the sliding distance observed in nacre tensile specimens, and therefore no significant hardening could be generated by the polymer during the tensile deformation of nacre. In the simple shear test, however, the shear strains at the interface are much higher and the polymer may contribute to the hardening observed at the macroscale.

Another nanoscale mechanism is controlled by the nanoasperities on the surface of the opposed tablets, which may enter in contact and interact as the interface is sheared (Fig. 8b). This mechanism was proposed as a source of strength and hardening at the interfaces [17,44]. The strength of aragonite is sufficient for the nanoasperities to withstand contact stresses with very little plasticity [10]. How-

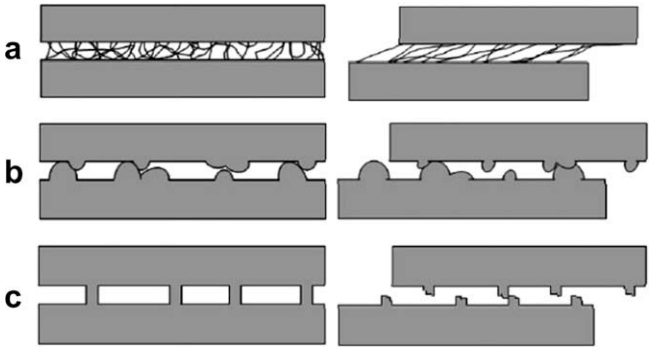

Fig. 8. Nanoscale mechanisms controlling the shearing of the tablet's interfaces: (a) biopolymer stretching; (b) aragonite asperities contact; (c) aragonite bridges initially intact (left), and then showing some potential relocking after shearing (right). Adapted with permission from [47].

ever, the small size of these asperities restricts the range of sliding over which they provide hardening to about 15–20 nm [44], which is much smaller than the sliding of 100–200 nm observed experimentally. Beyond sliding distances of 15–20 nm, one must therefore assume that the resistance provided by nanoasperities remains constant (as shown in [44]).

The third nanoscale mechanism at the interface is associated with the aragonite bridges (Fig. 8c). These bridges may act as reinforcements for the interfaces, and probably influence the overall behavior of nacre [46]. However, given the brittleness of aragonite, they could not generate much resistance to tablet sliding after failure, which probably occur at small interface shearing strains. After some sliding distance another mechanism was suggested, where broken bridges re-enter in contact, thereby generating re-locking of the tablets (Fig. 8c [47]). This mechanism has, however, not yet been demonstrated.

While the three nanoscale mechanisms described above contribute to the shearing resistance of the tablet interfaces, they cannot generate the level of hardening required for the spreading of non-linear deformations observed at the macroscale. In addition, none of these mechanisms could generate the transverse expansion associated with shearing of the layers (Fig. 7c).

A fourth mechanism was proposed by us where the hardening mechanism is generated by the waviness of the tablet surfaces [19,43]. As the layers slide on one another, the tablets must climb each others waviness, which generates progressive tablet interlocking and an increasing resistance to sliding. In addition, such mechanism could generate the observed transverse expansion, while the organic glue and bridges within the tablet cores maintain the tablets together. While this mechanism can easily be envisioned in simple shear (Fig. 7d), it is less obvious in tension, because tablet sliding only occurs in the tablet overlap areas. Close examination actually reveals that waviness also generated locking in tension. Fig. 9a shows an actual image of the structure of nacre. Tablet waviness is evident, and it can be seen that it generates dovetail like features at the end of some tablets. Such structure, loaded in tension, will generate progressive locking and hardening at large scales (Fig. 9b). Microstructure based three dimensional finite element models have actually demonstrated that waviness is indeed the key feature that generates hardening in nacre [19,43]. Even though some of the nanoscale mechanisms of Fig. 8 are required to maintain cohesive strength between tablets, waviness is required for hardening. Such hardening mechanism has a significant impact on the toughness of nacre, as described in the next section.

In order to capture the micromechanics involved in the tensile deformation of nacre, a three-dimensional finite element model of the structure of nacre was created. The aim was to generate a representative volume element (RVE), whose overall mechanical response is representative of the behavior of nacre at the macroscale (Fig. 10a). For this reason a large number of tablets was included in the model, about 300 tablets over two layers, in order to capture the actual tablet shapes and arrangement. Periodic boundary conditions were imposed along all three directions [19,43]. The

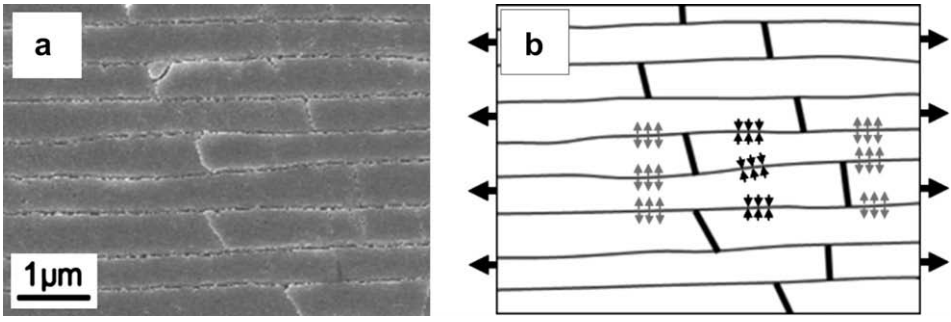

Fig. 9. (a) Scanning electron micrographs of a few dovetail like features at the periphery of the tablets. (b) Outline of the tablets contours, showing some of the stresses involved when nacre is stretched along the tablets. In addition to shear the interface is subjected to normal compression (black arrows) which generates resistance to tablet pullout. Equilibrium of forces at the interfaces requires tensile tractions at the core of the tablets. Reproduced with permission from [60].

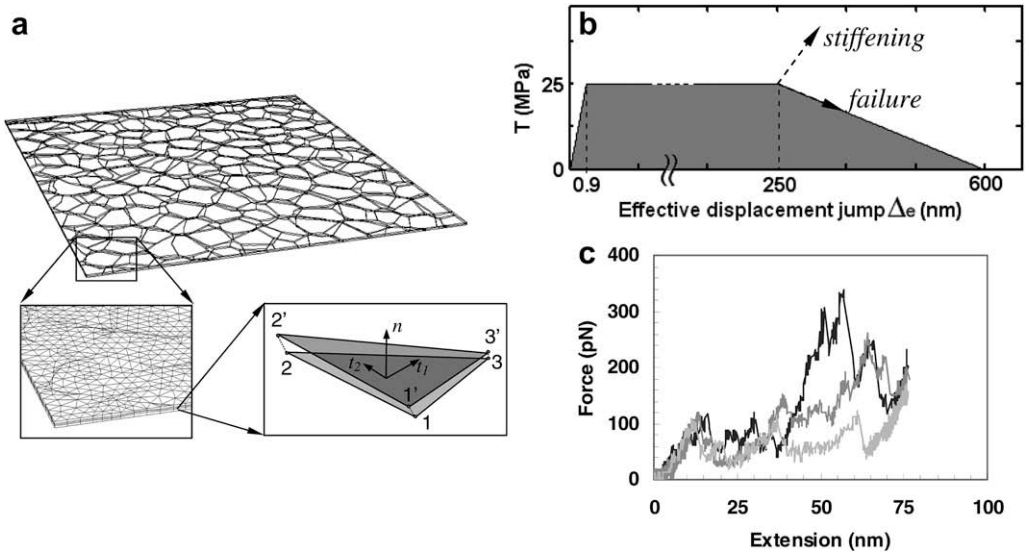

Fig. 10. (a) RVE model with cohesive interfaces. (b) Cohesive law implemented at the interfaces. (c) Experimentally obtained AFM pullout curve of some of the molecules that compose the biopolymer at the interface of nacre (reproduced with permission from [45]).

waviness of the tablets was obtained from actual micrographs of opposed cleaved faces of nacre (as in Fig. 5h) superimposed to recompose the arrangement of the tablets from one layer to the next [19]. The superposition was done by using features such as tablet layers steps or specimen corners, which can be accurately located on both cleaved faces (these features were not included to generate the RVE model). The tablets were modeled as transversely linear elastic, with parameters from single crystal aragonite, as measured by nanoindentation [10]. Following the crystallographic orientation of aragonite in nacre, the elastic constants along the [1 0 0] and [0 1 0] were averaged in the plane of the tablets to obtain $E_P = 106$ GPa, $E_Z = 82$ GPa, $\nu_P = 0.3$, $\nu_{ZP} = 0.06$, $G_{ZP} = 33.45$ GPa, where P indicates the direction in plane of the tablets and Z indicates the out of plane direction. In order to model the interaction between the tablets, cohesive elements [66–69] were inserted on the tablet's faces and sides. Tension and shear of the interface were assumed to be dominated by the stretching of biopolymeric chains. The mechanical response of the element was therefore controlled by the separation distance, or effective displacement jump across the interface. This displacement jump controlled the traction across the interface via the cohesive law (Fig. 10 a and b), which include both shear and normal components [19]. In order to prevent tablet interpenetration and to account for the interface thickness, its behavior in compression was modeled with interface parameters derived from compression experiments on nacre [10,19]. The main feature of the cohesive law is a constant cohesive strength over a large sliding distance (no hardening, Fig. 10b), which is consistent with biomolecular unfolding at a constant load (Fig. 10c). It is worthwhile noting that while the cohesive elements have zero thickness, the actual thickness of the interface was included in the derivation of their stiffness. The parameters of the cohesive law (initial slope, strength) were determined from compression and simple shear experiments [19]. The end of the plateau region was set to 250 nm, which is the maximum tablet separation observed on post-mortem tensile specimens. At this point the biopolymer could either stiffen or progressively fails (Fig. 10b). While this is an important feature of the cohesive law, this stage was never reached in the tensile RVE simulations (the maximum computed tablet separation was 180 nm). This cohesive law, while mostly based on macroscopic measurements, includes in a homogenized sense all the nanoscale mechanisms present at the interface: deformation of the confined biopolymer and nanoasperities contact interactions. More sophisticated cohesive formulations (not discussed here) were also used to capture specific features associated with the biopolymer constitutive response [50].

In order to investigate the effect of tablet waviness on the overall response of nacre, a "flat" model was generated with perfectly flat tablets (no roughness), and a "wavy" model was generated by directly implementing the surface topology measured by profilometry (Fig. 5h). To simulate macroscopic uniaxial tension the RVE was stretched until the model ceased to converge, which was associated with instability and actual failure of the material in tension.

The simulations showed that the model with flat tablets rapidly lead to localization of deformations and premature failure of the model (Fig. 11a and c). This confirms that while a material capable of maintaining cohesion over large displacements is necessary at the interface, it is not sufficient to provide the required hardening. A small amount of inelastic deformation was still observed, which was attributed to the tablet overlap statistics captured by the model. On the other hand, when tablet waviness was included, the strength and hardening observed experimentally was captured by the model (Fig. 11a, b, and d). This demonstrates that even without hardening at the local (nano) scale, hardening is generated by the waviness of the tablets. Some of these microscale features can readily be observed on micrographs of nacre. Fig. 11b shows a typical cross section, with the waviness of the tablets generating a geometry that resembles a dovetail. Such hardening feature is also present in the RVE model, as a natural outcome of using real tablet contours and waviness. Pulling the tablets apart generates significant compressive stresses across the tablets in the sliding areas, which impedes tablet separation. *This mechanism is sufficiently strong to spread inelastic deformations throughout the representative volume element and to generate hardening at the macroscale.* These simulations therefore demonstrated that waviness is an essential ingredient in the hardening mechanism of nacre. The implications on its fracture toughness are explored next.

2.4. Fracture of nacre

Many flaws are present within nacre, for instance, porosity and defective growth, Fig. 12. These flaws are potential crack starters that can eventually lead to catastrophic failure under tensile loading

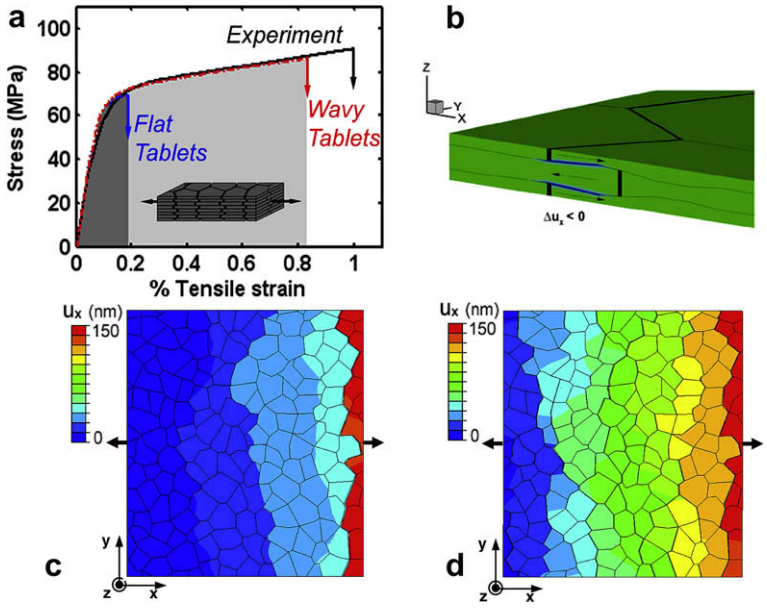

Fig. 11. (a) Tensile stress–strain curves from experiment along the tablets, and from RVE models with and without waviness. (b) Model of nacre showing dovetail geometries. (c) Displacement contours (along the *x*-axis) showing early deformation localization for the flat tablets case. (d) Deformation spreading throughout the RVE for the wavy case (the RVE strain is 0.2% for both c and d).

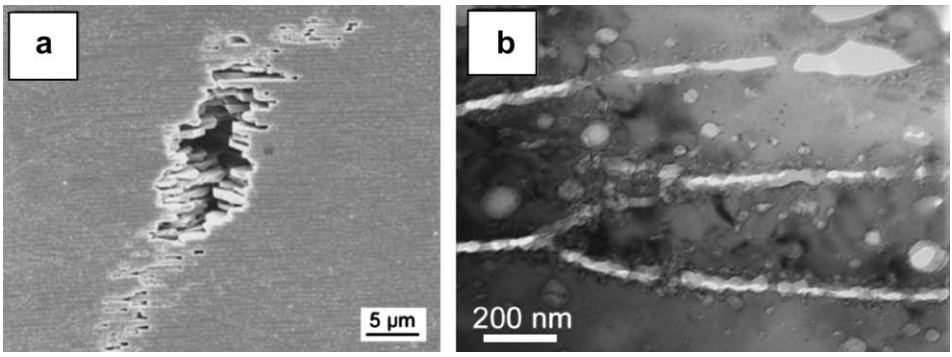

Fig. 12. (a) Large defect inside the nacreous layer (SEM). (b) "Stacking fault" in the tablet layers (TEM).

[70]. For a material like nacre defects cannot be eliminated so the only alternative is to *incorporate robustness* in the material design such that cracks that might emanate from them are resisted. The resistance to cracking can be assessed with fracture testing [1,16]. However it is only recently that the full crack resistance curve (toughness as function of crack advance) was determined for nacre from red abalone [60] (Fig. 13).

As the far field stress is increased on the fracture specimen, a white region appears and progressively increases in size (Figs. 13a and b) with the crack embedded in the region and trailing its boundary. The mechanistic details of this region were revealed by scanning electron microscopy postmortem observations. Fig. 13d shows the microstructure along a strip starting at the crack surface. Tablet sliding and interface openings (voids) over many rows of tablets are observed. Note that the magnitude of the opening decreases slightly with distance for the crack surface. These voids produce light scattering, which results in the white region observed during optical microscopy.

In the literature dealing with fracture mechanics, such inelastic region is referred to as *process zone* [70]. The process zone reached about 1 mm in width (Fig. 13b) when the crack started to propagate at a J-integral value of $J_0 = 0.3$ kJ/m^2, which is already 30 times higher than the toughness of pure aragonite ($\approx$0.01 kJ/m^2). During the fracture test the crack propagated slowly in a very stable fashion that

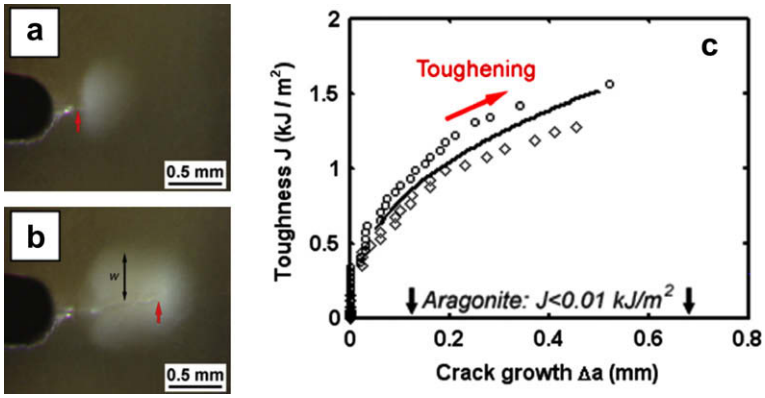

Fig. 13. (a) Prior to crack advance a tablet sliding zone develops ahead of the crack tip. (b) As the crack advances it leaves a wake of inelastically deformed material (a and b: optical images; red arrow shows location of crack tip at the onset of crack propagation and the steady state regime). (c) Crack resistance (J_R) curves for nacre from two experiments [60]. (d) SEM pictures of the damaged zone. The tablets sliding leads to openings at multiple tablets interfaces: the damage is spread far from the main crack (For interpretation of the references to colour in this figure legend, the reader is referred to the web version of this article.).

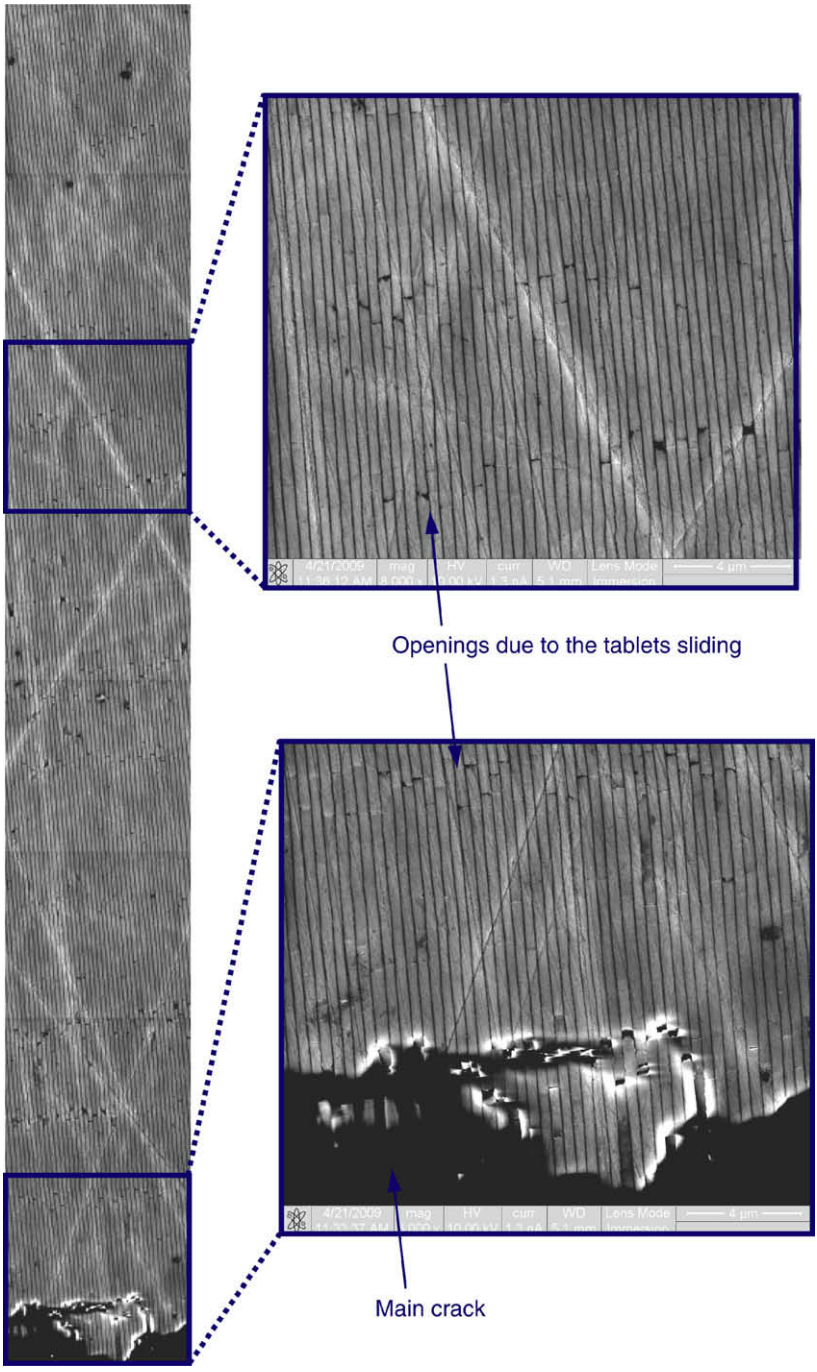

Fig. 13 (*continued*)

resembled tearing rather than the fast, catastrophic crack propagation typical to ceramics. The crack resistance curve is shown in Fig. 13(c), which shows that toughness increases significantly with crack advance Δa. Such rising crack resistance curves have also been observed in dentin enamel [71] and bone [72]. Cracks in such materials tend to be very stable; upon propagation they tend to slow down and can even be arrested. The rising crack resistance curve and high toughness of nacre was associated with the formation of the large, whitened region of inelastic deformation around the crack using fracture mechanics models [60].

By considering the energy dissipated upon an incremental crack extension or by straight use of the J-integral definition one can show that in the steady-state the initial (intrinsic) toughness J_0 is augmented by an energy dissipation term [70]:

$$J_{ss} = J_0 + 2\int_0^w U(y)\mathrm{d}y \tag{1}$$

where w is the process zone width and $U(y)$ is the energy density, *i.e.*, the mechanical energy (including dissipated and stored energies) per unit area per unit thickness in the z-direction, behind in the wake as $x \to \infty$ [73]. The analysis shares similarities with toughening in rubber toughened polymers [74,75] and toughening in transforming materials [73]. The exact calculation of $U(y)$ from strain fields requires accurate knowledge of the material constitutive law under multiaxial loading, including hysteretic unloading. Currently such constitutive description is only partially available for nacre. An estimate of the increase in J, in the *steady-state*, can be obtained, however, if one assumes that (i) the inelastic deformation associated with tablet sliding is the prominent energy dissipation and toughening mechanism (*i.e.*, the effects of shear and transverse expansion in the wake, as well as elastic energies trapped outside of the wake are negligible); (ii) the stress σ_{yy} around the tip can be predicted from the uniaxial tensile response (Fig. 7a); and (iii) the residual strain ε_{yy} in the wake decreases linearly from the crack face to the edge of the wake, as suggested by experimental observations. Then, the total J (Fig. 14) can be written as,

$$J_{ss} \approx J_0 + 2\int_0^w \int_0^{\varepsilon_{yy}(y)} \sigma(\varepsilon)\mathrm{d}\varepsilon\, \mathrm{d}y \tag{2}$$

The upper bound of the inner integral, $\varepsilon_{yy}(y)$, is the residual strain across the direction of the crack at $x \to -\infty$ (which decreases linearly with y). The integration of the loading–unloading histories across the width of the wake ($2w$ = 1 mm) yields an increase of toughness of 0.75 kJ/m^2. Combined with the initial toughness, the predicted steady state toughness is therefore 1.05 kJ/m^2. This value is lower than the experimental maximum toughness, of about 1.6 kJ/m^2, but shows that dissipative energies associated to elastic deformation, tablet sliding and associated dilation of the material are significant contributors to the toughening of nacre. In comparison, the contribution of other mechanisms such as crack deflection or crack bridging [76–78] are negligible. Note that this type of toughening is made

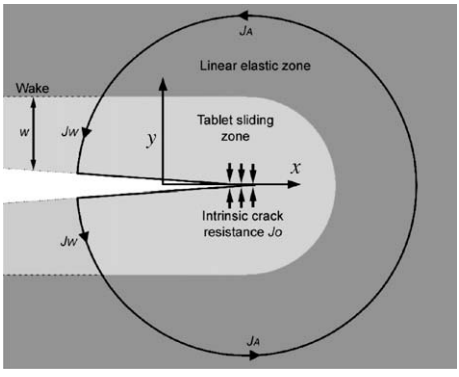

Fig. 14. Schematic showing the J contour used in the model (adapted from [70]).

possible by (i) spreading of nonlinear deformations and (ii) its associated energy dissipation. Advances in the constitutive description of nacre accounting for anisotropic inelastic effects will make possible a better quantification of J_{ss}.

In order to gain additional insight into the details of the toughening mechanisms operating in nacre, three-dimensional numerical simulations of the fracture process at the microstructural level would be useful. Unfortunately, such simulations are extremely expensive because they require three-dimensional microscopic details over the entire process zone, which is several millimeters in size. As an intermediate step between the analytical model and a full three-dimensional model, a two-dimensional microstructure-based fracture model of nacre was developed. The model was generated based on a composite image of about fifty scanning electron microscopy images of polished nacre from red abalone (Fig. 15a). The size of the model was 85 μm by 155 μm, and the orientation of the model was set so that the crack propagates across the tablet layers. The actual tablet contour was used to generate a "wavy" model (Fig. 15b), and a "flat" model was generated by straightening the interfaces (Fig. 15c). Two-dimensional versions of the cohesive elements used in the three-dimensional RVE were inserted between the tablets. The model, although of significant size, is still smaller than the process zone, and for this reason far field displacements could not be applied on the boundary. Instead, displacements measured experimentally using digital image correlation (Fig. 15d) were prescribed as boundary conditions on the model. These displacements were progressively increased, following the experimental measurements.

Fig. 16 shows the amount of tablet sliding ahead of the crack tip at increasing J values for both wavy and flat models. As J was increased, a clear difference appeared between flat and wavy models. In the flat model, tablet opening was significant and mostly localized in the plane of the crack. The final frame shows an actual crack (displacement jump > 600 nm) propagating across the model. On the

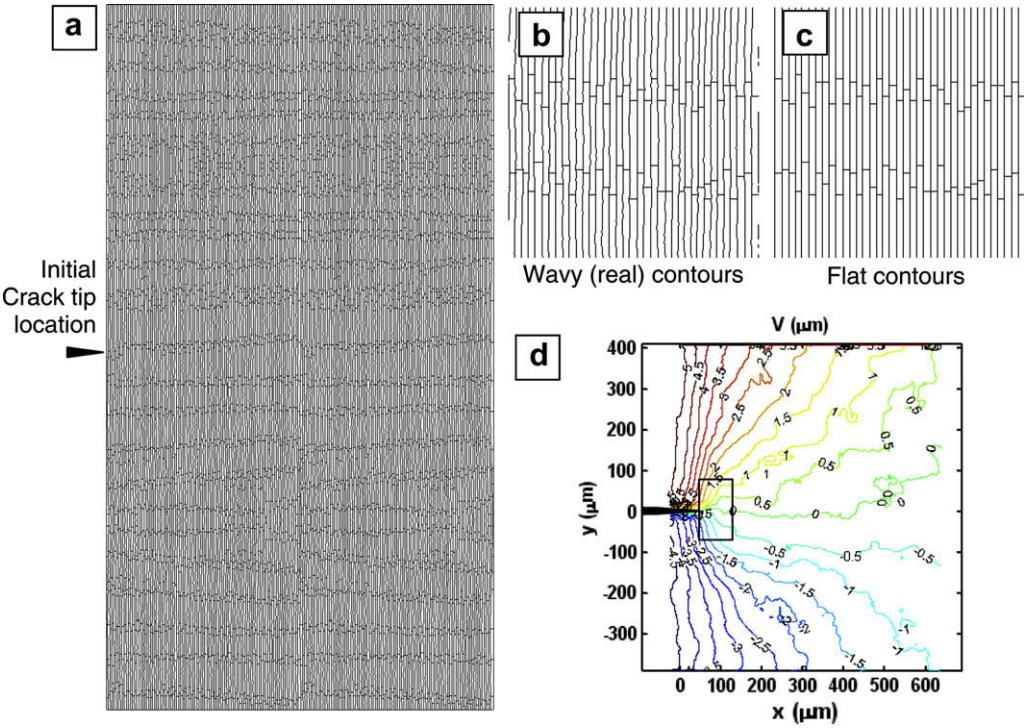

Fig. 15. (a) Two dimensional finite element model of nacre based on actual SEM images. (b) Detail of the wavy model. (c) Detail of the flat model. (d) Experimental vertical displacements around a crack advancing in a nacre specimen. The rectangle shows the size of the finite element model.

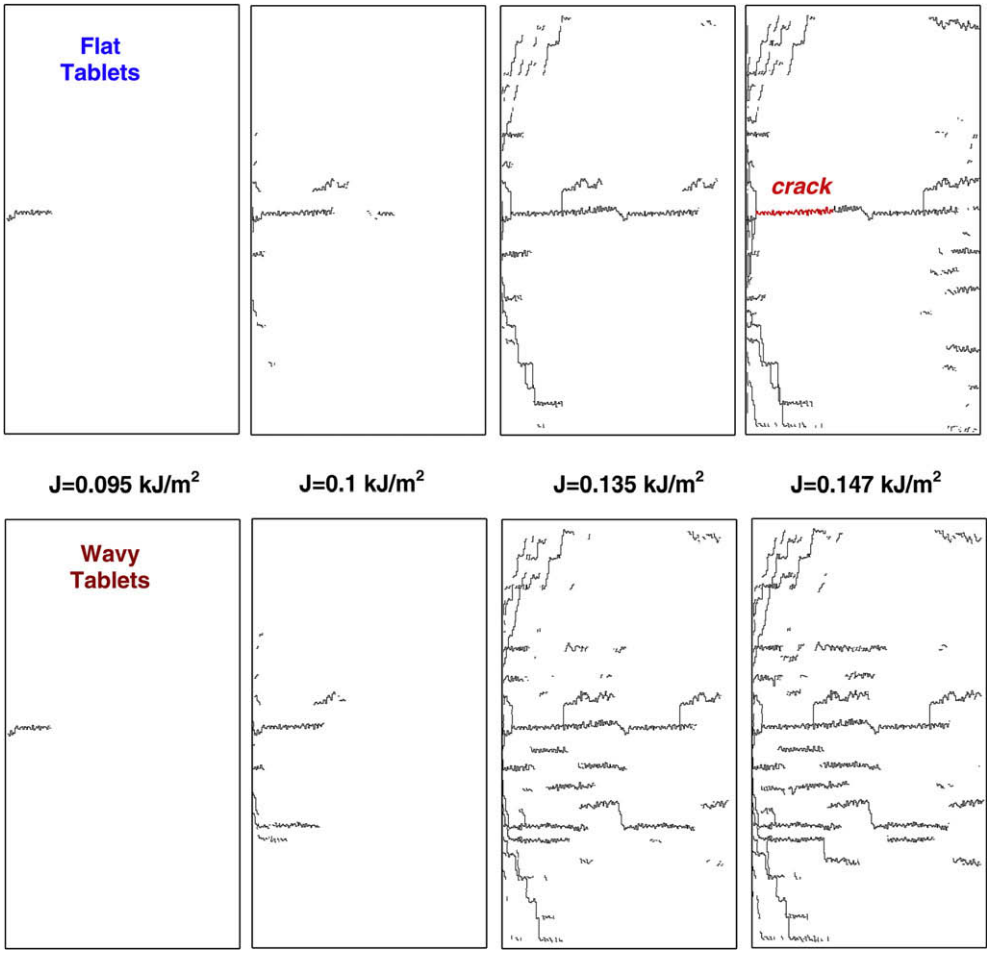

Fig. 16. Evolution of tablet opening for increasing applied J for flat and wavy models. The black lines highlight the interfaces for which the displacement jump is greater than 20 nm. The red lines highlight the interfaces for which the displacement jump is greater than 600 nm (For interpretation of the references to colour in this figure legend, the reader is referred to the web version of this article.).

other hand, the wavy model resisted cracking by spreading the inelastic deformation over an increasingly large region. The simulations highlight the role of tablet waviness as a requirement to spread inelastic deformations around cracks, which in turn result in crack extension toughening.

2.5. Other biological and natural materials

The discussion of nacre in the previous sections revealed important general characteristics of biological materials, which are found broadly in many other materials. The most notable feature of biological materials is that they form hierarchical structures, formed through self-assembly of smaller-scale constituents. Exploiting this general feature, the use of self-assembly to form hierarchical materials, for engineering material design remains a great challenge and opportunity of current materials research. In this section we briefly review structures of other mineralized biological tissues and organisms and point out the relation between structure and properties.

2.5.1. Structure of bone and associated deformation and fracture mechanisms

One of the most intriguing materials found in Nature is bone, a material composed out of assemblies of tropocollagen molecules and tiny hydroxyapatite crystals, forming an extremely tough, yet lightweight material [79,80]. Bone has evolved to provide structural support to a variety of organisms, and therefore, its mechanical properties are of great physiological relevance. Fig. 17 shows the hierarchical structure of bone, showing its seven hierarchical levels, and their relation to the mechanisms associated with mechanical deformation [79]. It is noted that bone is a very complex biological material, and currently we are only at the beginning of understanding quantitatively how this material deforms, fails and breaks and what type of mechanisms operate at various structural length- and time-scales. However, the advent of multi-scale experiments and novel theoretical and computational tools now enables the analysis of bone as a "material" with rigorous physical science techniques and great advances in the understanding of bone are expected in the years to come.

The basic building blocks of bone are collagen protein filaments and hydroxyapatite mineral crystals, which form so-called level 1 bone. These two constituents form the major structural ingredients in bone, together with a few non-collagenous proteins. The smallest scale hierarchical features of bone include the protein phase composed of tropocollagen molecules, collagen fibrils as well as mineralized collagen fibrils, referred to as level 2 bone. The collagen phase provides elasticity and the ability to dissipate energy under mechanical deformation. In the following paragraphs we provide a detailed description of the different levels and material components found in bone.

Collagen is one the most abundant proteins on Earth, forming a fibrous structural protein with superior mechanical properties. In addition to its importance in bone, collagen is universally found in many other biological materials, where it plays an important mechanical function. Other collagen-based materials include tendon, cartilage, skin, and the eye's cornea. Collagen is thus arguably the most

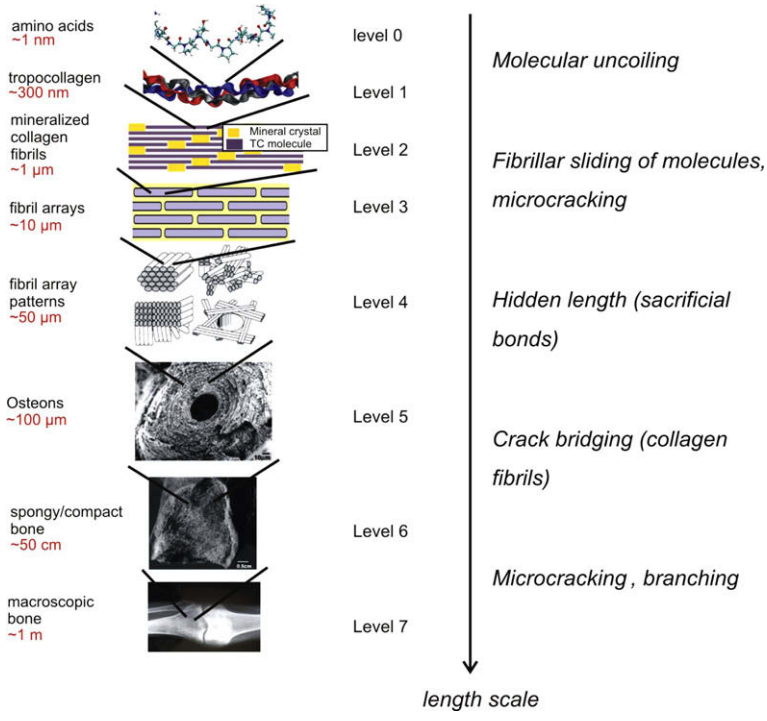

Fig. 17. Hierarchical multi-scale structure of bone, showing seven hierarchical levels, and their relation to the mechanisms of mechanical properties (inlays in level 4–7 bone reprinted with permission from Weiner et al. [79]). The left panel shows the characteristic structural features; the right panel indicates associated deformation and toughening (fracture resistance) mechanisms.

important structural protein in biology with multiple functions, and has been studied extensively in the past decades. Whereas early studies of collagen were focused on structural characterization, investigations in recent years increasingly focused on mechanical properties and their relation to biomedical processes and properties. Collagen consists of triple helical tropocollagen molecules (as shown in Fig. 18) that universally have lengths of approximately 300 nm (found across many species and types of collagen tissues) with a diameter of approximately 1.5 nm. Each tropocollagen molecule consists of a characteristic spatial arrangement of three polypeptides in a triple helical "nanorope" geometry, stabilized by H-bonding between different residues. Every third residue in each of these molecules is a glycine (GLY) amino acid, and about one fourth of the tropocollagen molecule consists of proline and hydroxyproline. The structure of collagen has been known since classical works focusing on the development of models that showed how tropocollagen molecules are stabilized by H-bonds [81] (see Fig. 18a, right panel, yellow dashed lines represent H-bonds). Severe mechanical tensile loading of collagen is significant under physiological conditions in various related tissues, representing one of its key performance features, as shown by its ability to stretch up to 50% tensile strain before breaking (under significant stiffening of the tangent modulus from zero to a few hundred MPa below 5% strain, 3–6 GPa at 10% strain, and up to 50 GPa immediately before rupture beyond 30–50% strain) while reaching force levels of more than 10 nN (per molecule), or 10–20 GPa stress (obtained by normalization of the force by the cross-sectional area of the molecule) [22,82–85]. Fig. 18b shows a tensile test of a tropocollagen molecule for deformation up to 40% strain. The plot also shows the progression of H-bond breaking as the molecule unravels [85]. Thereby, the breaking of H-bonds between 10 and 20% strain provides a

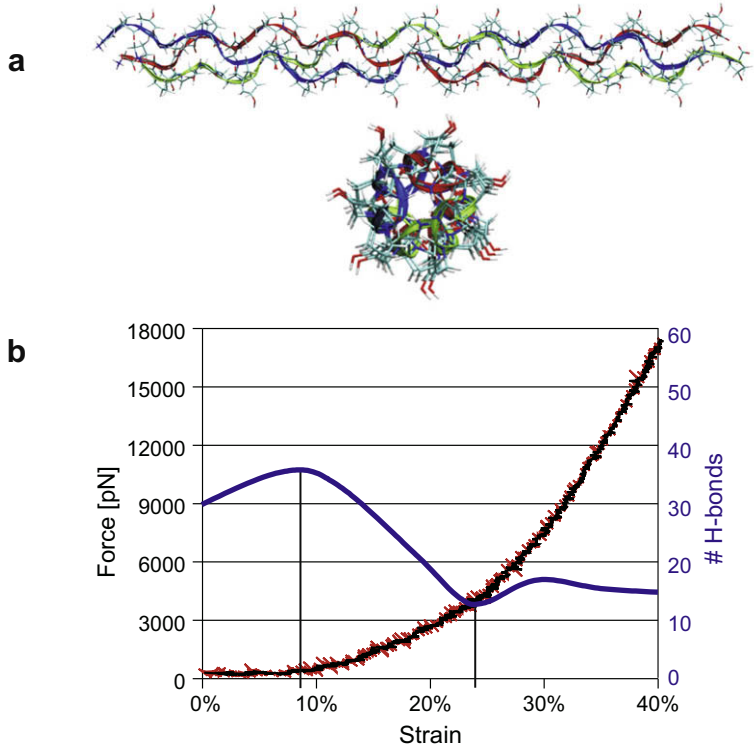

Fig. 18. Structure and nanomechanics of a triple helical tropocollagen molecule, the basic protein building block of bone. Subplot (a) shows the structure of this protein molecule; in the right plot the H-bond structure is depicted via the yellow thick dashed lines. Subplot (b) depicts the force-extension behavior, here shown up to 40% strain [85]. The plot also includes an indication of the number of H-bonds. (Left part of subplot (a) reprinted with permission from Bhattacharjee and Bansal) (For interpretation of the references to colour in this figure legend, the reader is referred to the web version of this article.).

major mechanisms that mediates deformation. The breaking of H-bonds is the basic mechanism that mediates large deformation of collagen fibrils, until the protein's backbone is being stretched and eventually ruptures; breaking of H-bonds is a reversible process and may thus provide a mechanism to dissipate energy through large-deformation behavior of the soft collagen matrix of bone.

At larger length-scales, staggered arrays of tropocollagen molecules form collagen fibrils, which arrange to create collagen fibers. Collagen fibrils are of particular significance for bone as they provide the structural template for bone formation. During bone formation, these fibrils become mineralized, when tiny mineral crystals of some form of hydroxyapatite form in the gap regions of the collagen fibrils, growing as the bone tissue becomes more mature. These mineralized collagen fibrils are highly conserved nanostructural building blocks of bone. The mineral crystals grow to sizes of a few tens of nanometers, but remain very thin (1–2 nm) in the out-of-plane direction. Arrays of fibrils, connected by a protein phase that provides additional dissipative properties, form fibril arrays referred to as level 3 bone. From level 0 to level 3 bone, different bone types feature a remarkable universality in their structural appearance. In other words, the smallest structural features in bone appear universally across species and for many different bone types. Fibril arrays in random, parallel, tilted or woven orientations form various fibril array patterns in level 4 bone. The bundled fibrils form collagen fibers which are organized at microstructural length-scales into a lamellar structure with adjacent lamellae being between 3 and 7 μm thick [86]. A characteristic cylindrical structure called osteons forms level 5 bone, providing a mechanism for constant remodeling of bone tissue (also referred to as Haversian systems). These structures are up to 200–300 μm diameter, composed of large vascular channels (~50–90 μm diameter) and are surrounded by circumferential lamellar rings, with so-called "cement lines" at their outer boundaries. The osteons contain cells that provide the ability to dissolve and renew bone, which provides adaptability to the structural properties. The bone remodeling process is crucial for bone properties, illustrating that bone is by no means a static material. Instead, it is a highly dynamic, "living" material that constantly changes its structure. This must be considered in understanding the mechanical properties of bone tissue, and its characterization within existing materials science concepts (primarily used for the analysis of "dead" materials) remains a challenging topic. Larger-level structures of bone (levels 6 and 7) include the characterization as spongy or compact bone and the overall structural shape of bone in our body.

Fig. 19 shows a nanomechanical analysis of bone deformation, along with structural mechanistic details of the associated deformation mechanisms. This result was obtained by a combination of molecular dynamics simulation and theoretical analysis, where it has been shown that the characteristic nanostructure of mineralized collagen fibrils is vital for its high strength and its ability to sustain large deformation, as relevant to the physiological role of bone, creating a strong and tough material. Fig. 19a plots the stress–strain response of a pure collagen fibril compared with that of a mineralized collagen fibril, under tensile loading, for tensile strains up to 50%. The stress–strain responses for both structures are qualitatively and quantitatively different, indicating that precipitation of hydroxyapatite crystals during bone formation significantly alters the material response. The mineralized collagen fibril features a larger strength and much increased energy dissipation under deformation. Plastic deformation starts at approximately 6.7% tensile strain for the mineralized fibril, whereas it occurs at approximately 5% tissue strain in the case of a pure collagen fibril. Further, the mineralized collagen fibril shows significant softening at larger strains, with a characteristic saw tooth shaped stress–strain curve due to repeated intermolecular slip. The mineralized fibril features a higher stiffness than the pure collagen fibril. Fig. 18b and c show snapshots of the molecular geometry under increasing tensile load, clearly showing the deformation mechanism of intermolecular slip. Fibrillar yield is characterized by intermolecular slip (see red circle highlighting a local area of repeated molecular slip). Slip leads to formation of regions with lower material density, as can be seen in the images.

This analysis of the molecular mechanisms of protein and mineral phases under large deformation of mineralized collagen fibrils revealed a fibrillar toughening mechanism that leads to a manifold increase of energy dissipation compared to fibrils without mineral phase. This fibrillar toughening mechanism increases the resistance to fracture by forming large local yield regions around crack-like defects, a mechanism that protects the integrity of the entire structure by allowing for localized failure. As a consequence, mineralized collagen fibrils are able to tolerate micro-cracks on the order of

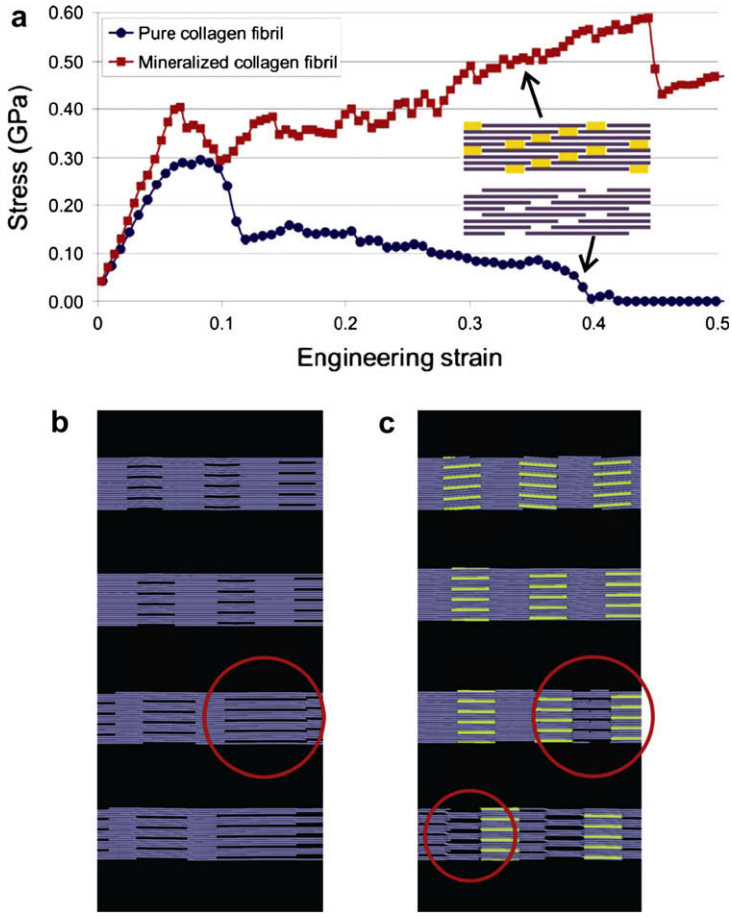

Fig. 19. (a) Computational result of the stress–strain response of a mineralized versus unmineralized collagen fibril, revealing the significant effect the presence of mineral crystals in collagen fibril has on the mechanical response [42]. (b) Snapshots of the deformation mechanisms of collagen fibrils, and (c) mineral collagen fibrils. Slip initiates at the interface between mineral particles and tropocollagen molecules. Repeated occurrence of slip reduces the density, leading to formation of nano-scale voids.

several hundred micrometers size without causing any macroscopic failure of the tissue, which may be essential to enable bone remodeling. The analysis proves that adding nanoscopic small platelets to collagen fibrils increases their Young's modulus, yield strength as well as their fracture strength. It is found that mineralized collagen fibrils have a Young's modulus of 6.23 GPa (versus 4.59 GPa for the collagen fibril), yield at a tensile strain of 6.7% (versus 5% for the collagen fibril) and feature a fracture stress of 0.6 GPa (versus 0.3 GPa for the collagen fibril).

Other deformation and fracture mechanisms exist in bone at larger hierarchical levels, including the breaking of sacrificial bonds between mineralized fibrils, the formation of microcracks, crack bridging (via collagen fibrils arranged orthogonal to the crack), and the formation of larger plastic zones around crack tips that contribute to an increase in bone's overall toughness [87–89].

2.5.2. Universality and diversity in biological materials

Even though protein materials lead to vastly complex structures such as cells, organs or organisms with very different material properties, the fundamental material buildup shows striking similarity between seemingly very different materials. The analysis of the composition of biological materials

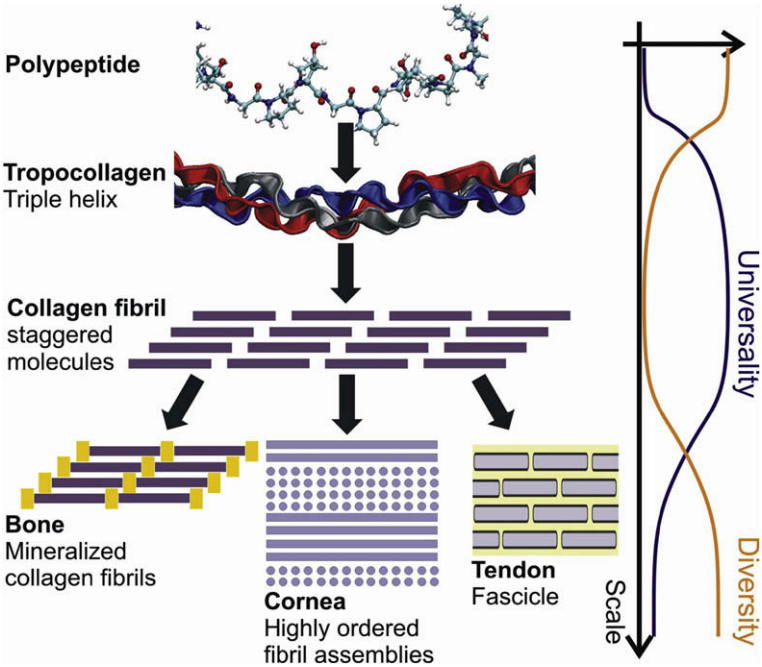

Fig. 20. Universality and diversity in the structure of collagen-based biological materials [119]. Beyond the fibril scale, structural features vary significantly, here shown for bone, cornea and tendon. This analysis reveals how biological materials with diverse properties are created through the use of universal features, a materials design paradigm that could be exploited also for the use synthetic materials [90].

has revealed that the underlying mechanisms of material formation that can be classified into two major categories, *universal* and *diverse* features [90]. Some of the structural features materials are commonly found in different tissues, that is, they are highly conserved and are classified as "universal". Examples of such universal building blocks include the triple helical tropocollagen molecule or the occurrence of collagen fibrils in various types of collagenous tissues (e.g., bone, tendon, and cornea). In contrast, other features are highly specific to tissue types, such as particular filament assemblies, beta-sheet nanocrystals in spider silk or tendon fascicles [91]. Fig. 20 displays the interplay of diversity and universality for collagen-based materials, plotted over characteristic length-scales. Universality is found predominantly at ultra-small scales, forming basic protein constituents or characteristic assembly patterns. It has been speculated that this universality is linked to mechanical robustness of the properties at nanoscale, a feature that is not limited to collagenous materials or bone, but that is found in many other biological protein materials [92]. A greater diversity of structures is typically found at larger length-scales, where it is established in the formation of particular fibril patterns (e.g., fascicles in tendon versus Mineralized collagen fibrils in bone). Recent research provides evidence that the occurrence of hierarchical structures is crucial to combine seemingly disparate properties such as high strength and high robustness, as they provide the structural basis to unify – in a single material – both universal (=providing robustness) and highly diverse (=providing functionality).

3. *De novo* synthesis of bioinspired or biomicking composite materials

The attractive mechanical properties of nacre, bone and other materials have inspired the development of a large class of biomimetic materials and organic/inorganic composites [93]. The creation of artificial shell materials with their intricate microstructure is a challenge that requires both the design of optimum microstructures and the development of fabrication procedures to implement these

designs. In the following section, we describe some of the efforts at mimicking the architecture of nacre with different fabrication methods. Other materials will be discussed subsequently, including a bone-mimicking metal nanocomposite structure and a case study of the design of novel filaments based on alpha-helical proteins.

3.1. Large scale "model materials"

It has been argued [94,95] that an important toughening mechanism of nacre is crack deflection due to the presence of relatively weak interfaces between the brittle aragonite tiles. Model systems on the macroscopic scale can utilize this toughening mechanism while circumventing the many challenges of mimicking the shell architecture at the μm level [94,95]. In this way, larger scale layered composites with ceramic tablets held together by weak interface "glue" are able to overcome the brittleness of ceramics.

Clegg et al. used thin squares tiles (50 mm × 50 mm × 200 μm) of SiC doped with boron [94]. The tiles were coated with graphite to retain a weak interface after sintering. Under a three point bending test, the crack is deflected along the weak interfaces, preventing catastrophic failure (Fig. 21a). The load–deflection curve in Fig. 21b shows the load continuing to rise after initiation of crack growth. Increases in toughness and work of fracture by factors of 5 and 100 over monolithic SiC were reported.

Another larger scale composite system used alumina tablets (length 2–3″, thickness 0.04″) for the ceramic phase [95]. The plates were bonded with thin adhesive transfer tapes at the interfaces, which exhibited exceeding resilience and extensive ligament formation (Fig. 21c). Fig. 21d shows the load–deflection curves of three sets of composite beams from four point bending tests. The composites with continuous layers and segmented layers with 82 vol % ceramic showed limited deflections before abrupt failure. However, the composite beam with 89 vol % ceramic exhibited an extensive deflection resulting in a toughness six times that of a monolithic alumina beam. In agreement with the above,

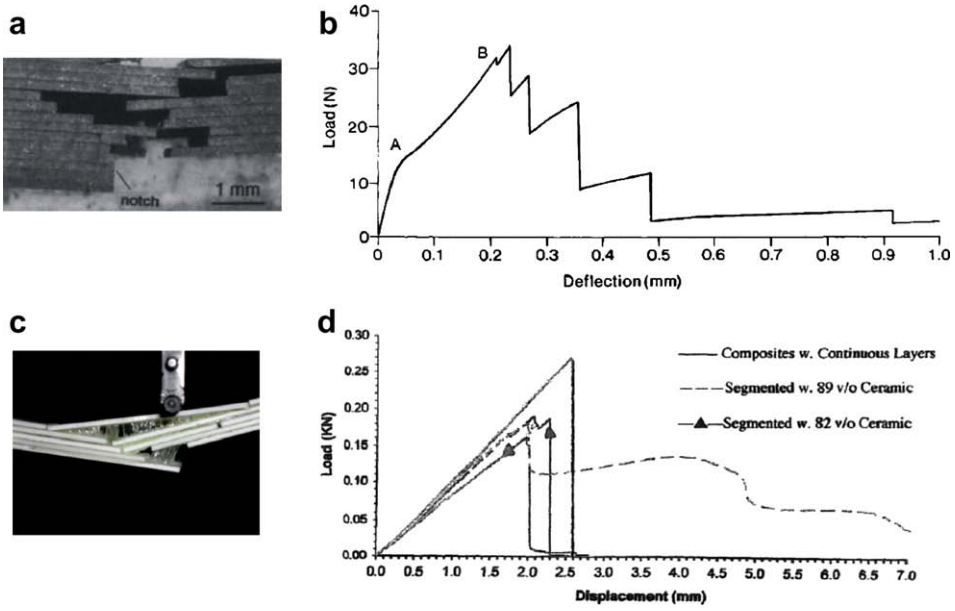

Fig. 21. (a) The fracture surface of a laminate composite specimen under three point bending. The role of the interface in deflecting cracks can be clearly seen. (b) The load–deflection curve of the specimen. Crack growth begins at A, and is followed by a rising load for further deflection till B when crack growth becomes more rapid. Reproduced with permission from [94]. (c) A beam being deflected in bending, showing tenacious ligament formation in the adhesive between the platelets. (d) Load–displacement curve from four point bending tests of laminated composites. Reproduced with permission from [95].

adhesives that were too strong led to brittle failure. High volume fractions of adhesive resulted in detrimental mechanical properties as well. The study indicates that a resilient and extensible interphase together with a segmented layered microstructure with an *optimal ceramic volume fraction* is required to achieve maximal toughening. However, due to the limited number of samples in the study, quantitative conclusions regarding the role of adhesive and layer segmentation in the crack deflection and bridging process have not been reported.

The toughening achieved by crack deflection in these macroscopic composites, however, is quite limited compared to that seen in nacre, which indicates that other mechanisms such as tablet locking and damage spreading plays an important role in the high toughness of nacre. Based on the deformation mechanisms identified by us (see Section 2), we designed a synthetic material with the microstructure shown in Fig. 22a. The design is directly inspired from the key features we identified from the microstructure of nacre: Tablets arranged in columns with some overlap, and tablet waviness (which are translated into dovetail-like locking features at the ends of the tablets, Fig. 22a). The mechanical response of this periodic composite was examined using an RVE defined by several non-dimensional geometric parameters: core length L_c/t, overlap length L_o/t, dovetail angle θ interface thickness h/t, and bridge diameter b_d/t (four cylindrical bridges, not shown in the figure, were placed in the core region). By performing detailed finite element analyses [96], we investigated deformation and failure modes of a composite material consisting of ABS for the tablets (a common rapid prototyping material) and BGEBA epoxy for the filler. Bounds in the design space defining the geometry of the microstructure were identified such that failure would result from tablet sliding, its spatial spreading, and finally tablet pullout rather than premature tablet fracture or localized cracking.

Based on the identified bounds, the composite material shown in Fig. 23 was designed, manufactured and tested. The measured stress–strain behavior (Fig. 22b) begins with an elastic response followed by tablet sliding when the strain exceeds approximately 1.3% (point A in Fig. 22b). Upon monotonic increases in prescribed displacement, sliding in the overlap region progresses even with a small drop in stress until failure occurs at about 2.3% strain (point F in Fig. 22b). Interestingly, a mild softening stage is followed by a hardening stage, beyond point C, until failure. The failure is trigger by fracture of the dovetail on a boundary tablet. Softening followed by hardening was also predicted by finite element analyses of the synthetic material [96]. Moreover, these simulations, based on periodic boundary conditions, reveal that larger samples would be able to exploit the full hardening phase and fail at much larger strains [96].

Digital image correlation of a sequence of images captured with a CCD camera and a macro lens (Fig. 23a) reveals that tablet sliding occurs at multiple locations. The phenomenon is clearly observed in a plot of displacement as a function of position along the sample at five levels of strain, Fig. 23b. At

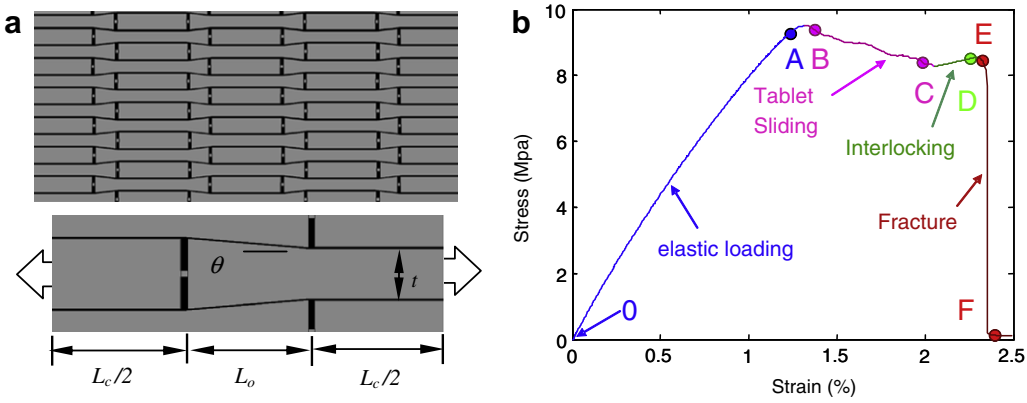

Fig. 22. (a) Microstructure of a synthetic material with wavy interfaces achieved by means of tablets with dove-tail morphology (top). RVE with characteristic dimensions (bottom). (b) Stress–strain behavior of a synthetic nacre made by rapid prototyping. Inelastic deformation, associate to tablet sliding and damage spreading, is observed prior to fracture.

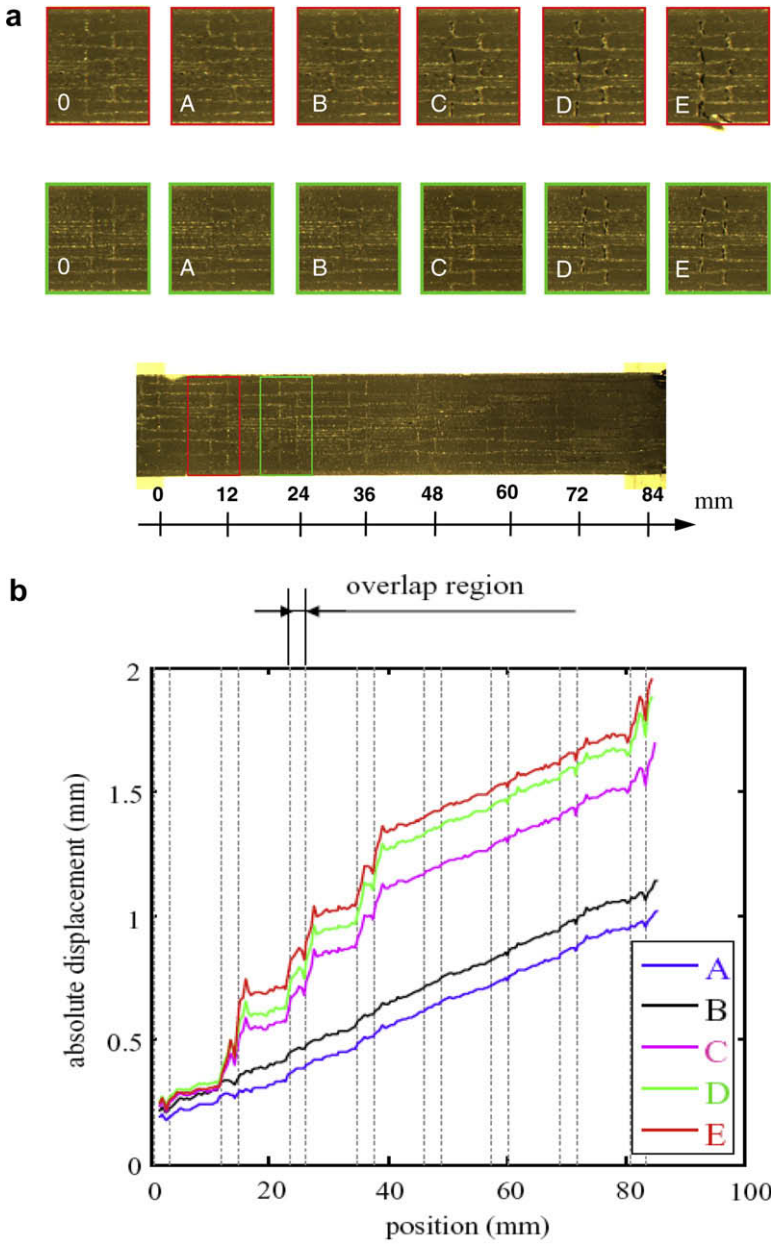

Fig. 23. (a) Sequence of images, at two regions of the sample, showing tablet sliding and spreading. (b) Displacement versus position plots as a function of deformation obtained from digital image correlation of images shown in (a).

state A, the deformation is homogeneous and consequently, the slope in the displacement-position curve is constant along the length of the sample. By contrast, at later deformation states, tablet sliding at four overlap regions are revealed by local changes in slope (Fig. 23b). These results confirm the role of tablet waviness on the capability of the composite to spread damage and consequently maximize

energy dissipation. *As such they constitute the first demonstration of nacre-like behavior, i.e., damage spreading under a macroscopic homogeneous tensile deformation field.* We have also performed tests on samples with geometries outside the identified bounds [96] and confirmed premature failure by tablet fracture just beyond the initial elastic response.

3.2. Ice templation

A novel method to develop layered-hybrid materials was developed by Deville et al. by utilizing the physics of ice formation [97]. By freezing concentrated suspensions containing ceramic particles using precisely controlled freezing kinetics, a homogenous, layered, porous scaffold could be built. The porous scaffolds were then filled with a second phase, either organic or inorganic, to fabricate dense layered composites.

The freeze-casting process involves the controlled unidirectional freezing of ceramic suspensions. While the ceramic slurry is freezing, the growing ice crystals expel the ceramic particles, causing them to concentrate in the space between the ice crystals (Fig. 24). The ice is then sublimated by freeze drying, leaving a ceramic scaffold with parallel layers as thin as 1 μm (Fig. 25a). The ceramic layers are quite homogeneous, and display a degree of segmentation. Interestingly, the process leads to spontaneous surface roughness and ceramic bridges between layers due to trapped particles between the ice dendrites, mimicking the asperities and mineral bridges of nacre. Note that a feature identified as key in the mechanics of nacre, conformal tablet waviness [19,43,50], is not present in the resulting scaffolds.

These porous scaffolds can be filled with a second phase, such as epoxy or Al–Si, to fabricate dense composites. The resulting layered composite structure exhibited extensive crack deflection due to delamination of the layers, leading to increased toughness. The fracture path of Fig. 25c clearly indicates the tortuous crack path around the ceramic phase, resulting in a "tablet-pullout" failure mode. However, the reported toughness of Alumina/Al–Si composite is about 5.5 MPa $m^{1/2}$; compared with the fracture toughness of aluminum oxide usually in the range of 3–5 MPa $m^{1/2}$, the increase in toughness is quite modest, possibly due to the overly weak interface. When the interface was modified by adding a small amount of Ti to the aluminum alloy, the fracture toughness was further increased to 10 MPa $m^{1/2}$. More recently, aluminum oxide and polymethyl methacrylate structures were made with toughness as high as 30 MPa $m^{1/2}$ [98]. The ice templation process allows a measure of control over the morphology of the inorganic layers and the chemistry of the interface, however, the attained volume fraction of the ceramic phase is low (about 45%) compared to nacre and control of morphological features such as tablet waviness have not been realized. In this sense, toughness improvements

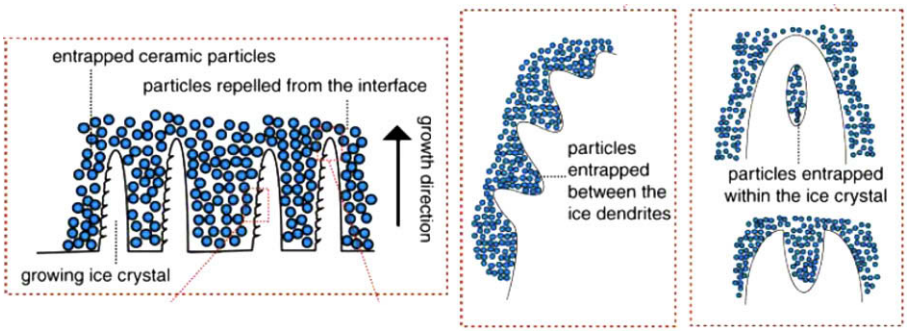

Fig. 24. Processing principles for ice templation. While the ceramic slurry is freezing, the growing ice crystals expel the ceramic particles, creating a lamellar microstructure oriented parallel to the direction of the freezing front. A small fraction of particles are entrapped within the ice crystals by tip splitting, leading to the formation of inorganic bridges and roughness on the walls. Reproduced with permission from [97].

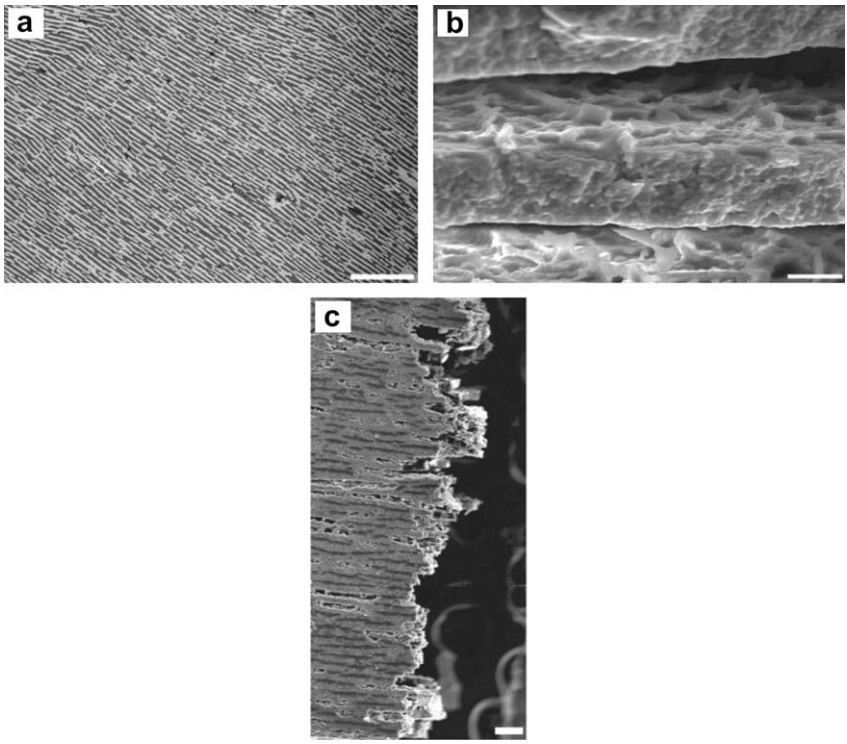

Fig. 25. (a) The layered microstructure of the IT dense composite (alumina–Al–Si composite). (b) The particles entrapped between the ice dendrites generate a characteristic roughness on the lamellar surface that mimics that of nacre. (c) Extensive crack deflection at the interface leads to tortuous crack paths. Scale bars are (a) 300 μm, (b) 10 μm, and (c) 100 μm. Reproduced with permission from [97].

are the result of mechanisms different to those observed in mollusk shells and much less well defined and quantified from a micromechanics viewpoint.

3.3. Layer-by-layer deposition

A more conventional approach is sequential deposition, or layer-by-layer assembly, which has been widely used to fabricate multilayered composites inspired by nacre. Several such efforts include the fabrication of multilayers of alternating hard and soft components, TiN/Pt, with an ion beam sputtering system, [99] and composites based on calcium carbonate (which is the mineral component of nacre in its aragonite phase [100,101]) through repeated calcium carbonate crystallization onto a film of charged molecules. Although improved hardness and toughness were reported for the TiN/Pt composite, [99] as with the self-assembly process, the composites formed via sequential deposition lack a segmented layered microstructure.

This limitation was overcome by Tang et al. [102] by layering Montmorillonite (MTM) clay tablets (C) and PDDA polyelectrolytes (P), by sequential adsorption. The process consists of P-adsorption, rinsing, C-adsorption, and rinsing; repeating this process n times results in the $(P/C)_n$ multilayers. The thickness of each clay platelet is 0.9 nm, and a multilayer with $n = 100$ has a thickness of 2.4 μm, three orders of magnitude smaller than the characteristic dimensions of nacre.

Strong attractive electrostatic and van der Waals interactions exist between the negatively charged clay tablets and positive polyelectrolytes; these forces orient the clay platelets parallel to the surface which results in a high degree of ordering of the microstructure with the clay sheets strongly overlap-

ping each other, as seen in Fig. 26. Note that the material microstructure exhibits layer waviness, but in contrast to nacre it appears somewhat random and uncontrollable during manufacturing.

Although the segmented layered composite structure is characteristic of that in nacre, the deformation behavior is quite different from that of nacre as can be seen from Figs. 7a and 27a. The layered composites displayed an abrupt hardening after an initial plastic deformation, due to the sacrificial noncovalent bonds of the PDDA molecules. The initial low stiffness region of $\varepsilon < 0.05$ is due to the disruption of the weak short-range van der Waals interactions in the initial tightly coiled configuration (Fig. 27c), after which hardening occurs as the stronger P–C ionic bonds are broken as the clay platelets slide over each other. The saw-tooth elasticity profiles of the macromolcules in Fig. 27b mimic those seen in nacre; [20] however, the passive role of the clay in deformation compared to that of the tablets in nacre leads to the difference in the macroscopic behavior.

Significant increases in stiffness and strength compared to the polymer phase is achieved, with the multilayers exhibiting high ultimate tensile properties of $\sigma_u = 100$ MPa and $\varepsilon_u = 0.08$. However, the

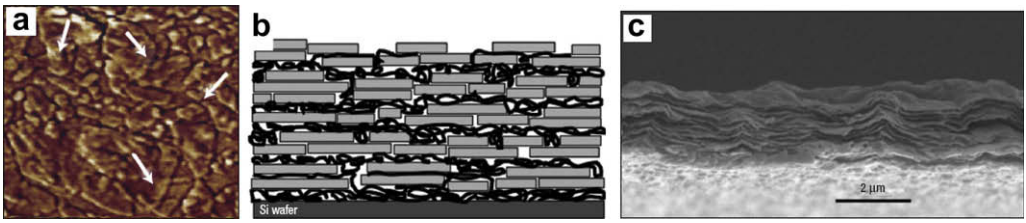

Fig. 26. The microscopic structure of the $(P/C)_n$ multilayers. (a) Phase-contrast AFM image of a $(P/C)_1$ film. The arrows mark the overlap of clay platelets. (b) A schematic of the $(P/C)_n$ structure. Note that n describes the number of deposition cycles rather than the number of layers, since several C–P layers may be deposited in each cycle. The thickness of each clay platelet is 0.9 nm. (c) SEM image of an edge of a $(P/C)_{100}$ film. Reproduced with permission from [102].

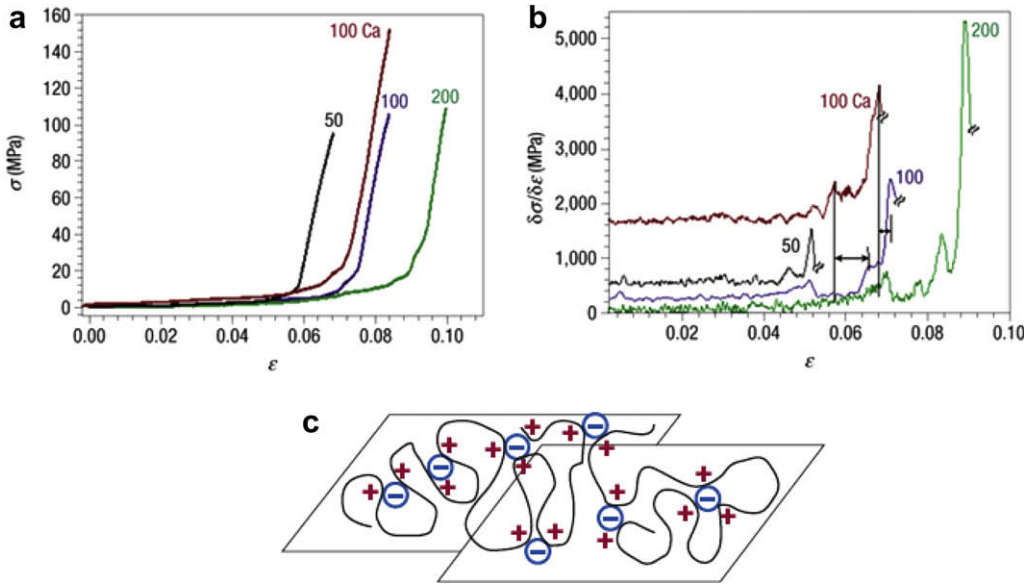

Fig. 27. (a) Stress–strain curves of free standing films $(P/C)_{50}$, $(P/C)_{100}$, $(P/C)_{200}$, and $(P/C)_{100}$ ion exchanged with Ca^{2+} ions. (b) The derivatives of the stretching curve revealing the saw-tooth pattern. (c) Polyelectrolyte folding and P–C ion pair formation. Reproduced with permission from [102].

improvement does not quite reach the expected theoretical strength of reinforced polymers [103]. In addition, the reliance on the strong attraction between the constituents limits the application of the method to a narrow range of materials.

In order to improve the load transfer from the polymer to clay tablets, thereby improving the mechanical properties of the composite, Podsiadlo et al. turned to tailoring the platelet-matrix interface chemistry [103,104]. Use of polymers that form stronger bonds with clay, such as DOPA (L-3,4-dihydroxyphenylalanine), which exhibit strong binding to clay as well as strong self-crosslinking in the presence of Fe^{3+}, and poly(vinyl alcohol) (PVA), which forms epitaxial hydrogen bonds and cyclic crosslinking to Al atoms on the MTM clay surface, resulted in dramatic increases in strength and stiffness as well as toughness. However, the increased stiffness of the matrix led to a decrease in the failure strain and brittle fracture at the same time. Further modification of the interface chemistry and corresponding further increases in strength and stiffness could be achieved by glutaraldehyde (GA) treatment, a crosslinking agent for PVA.

The LBL deposition method was also used by Bonderer et al. [105] to fabricate alumina–chitosan films, reinforcing the ductile chitosan polymer with the strong but brittle alumina platelets. By using alumina platelets rather than clay, the aspect ratio of the platelets could be optimized to maximize the load transfer while avoiding platelet fracture, according to the classic composite shear lag load transfer model. This favors a fracture mechanism by platelet pullout and matrix shear rather than platelet fracture, as seen in nacre.

The submicrometer-sized platelets, with a thickness comparable to that of nacre, could be strongly aligned and evenly dispersed in the chitosan matrix for up to 20% volume fraction, as seen in Fig. 28a. Note that this volume fraction is several folds smaller than that in nacre (~95%) resulting in a material with deformation mechanisms also very different. The mechanical properties of the composite under tensile loading exhibit significant increases in the stiffness and strength compared to the chitosan matrix, while retaining the plasticity of the chitosan (Figs. 27b). This indicates extensive shear deformation of the matrix before platelet pullout, due to the strong interface bonding.

Despite the combined strength and toughness exhibited by the alumina–chitosan films, the low inorganic volume fraction that could be achieved with the alumina–chitosan films means that the toughening arises mainly from the plasticity of the matrix, and is therefore limited compared to nacre. To realize the full potential of nacre-inspired composites, specifically the orders of magnitude increase in toughness, the contributions from the small length scale features of nacre, namely the close-packed tablets, and the nanostructure of the tablets such as mineral bridges and tablet waviness need to be captured. The high degree of control that this requires over the fabrication and arrangement of the composite microstructure still remains a highly challenging goal.

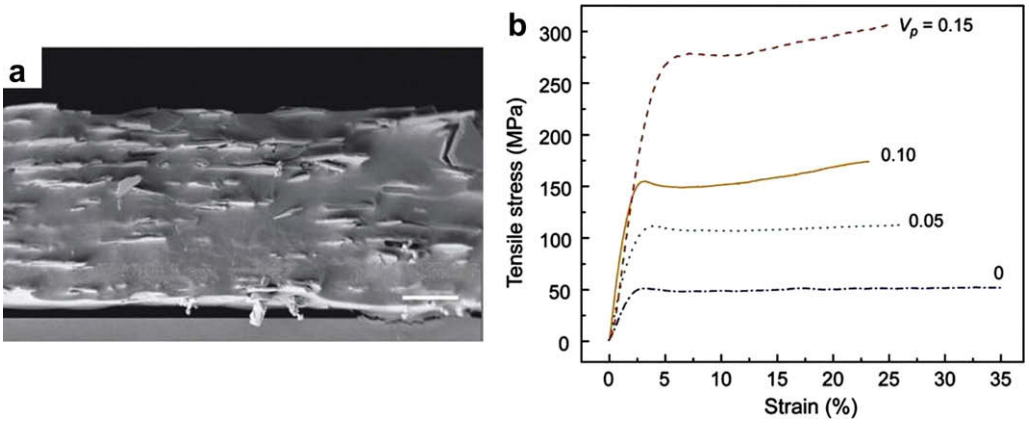

Fig. 28. (a) The microstructure of alumina–chitosan film for $V_p = 0.11$. (b) The tensile stress–strain curves for alumina–chitosan films with V_p up to 0.15. V_p = volume fraction of alumina. Reproduced with permission from [105]. 2008 AAAS.

3.4. Thin film deposition: microfabricated structures

While a lot of effort has been put into reproducing the layered structure of nacre, an attempt was made recently to mimic the crossed-lamellar microstructure of the Queen conch (*Strombus gigas*), using MEMS (microelectro-mechanical systems) fabrication processes [106]. The conch shell has a logarithmic spiral shape, and exhibits the highest level of structural organization among mollusc shells. The shell has a particularly high ceramic content of 99 wt %, composed of lath-like aragonite crystals arranged in a crossed-lamellar or ceramic "plywood" structure (Fig. 29). While nacre with the brick and mortar microstructure exhibits the highest tensile and compressive strengths among the various mollusc shell micro-architectures, the crossed lamellar structure is associated with the highest fracture toughness [106–108].

Polysilicon and photoresist were chosen as substitutes for aragonite and the organic matrix, and the microstructure was fabricated as a stack of three consecutively deposited films, as shown in Fig. 30. Each film is an approximation of the inner (or outer) and middle layers of the *S. gigas* shell; the lower half represents the inner layer with vertical interfaces, while the top half represents the middle layer with the interfaces oriented at ±45° to the horizontal. The films are deposited so that the angled interfaces are oriented in alternating directions designed to make the middle layer tougher than the inner layer.

The fabrication makes use of standard MEMS processing technology, repeating the deposition of a thin silicon film (~2 μm) on which trenches for the interfaces are etched out with RIE (reactive ion etching), which are in turn filled with photoresist. The use of MEMS processing enables a high degree of control over the morphology and the fabrication of large numbers of specimens, however at the expense of speed and cost. Results of mechanical tests performed as shown in Fig. 31, indicated that the micro-composite possesses significant ductility and toughness compared to monolithic silicon, with an estimated increase in energy dissipation of 36 times that for silicon. However, the energy-dissipation mechanisms were slightly different from those of the mollusc shell. Rather than the multiple tunnel cracking seen in the *S. gigas* shells, the micro-composite showed extensive delamination between

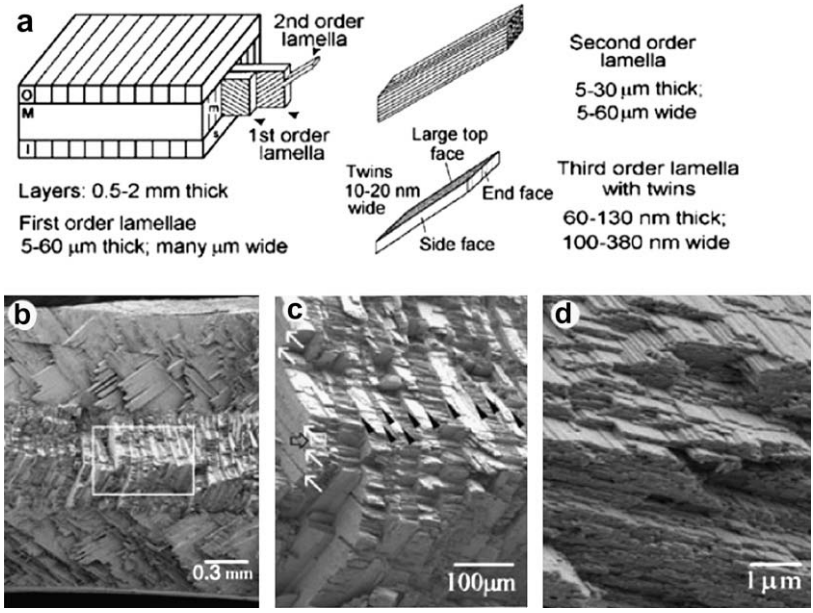

Fig. 29. Micro-architecture of the shell of *S. gigas*. (a) A schematic drawing of the crossed lamellar structure, with characteristic dimensions of the three lamellar orders. (b), (c) and (d) SEM images of the fracture surface of a bend specimen at increasing magnification. Reproduced with permission from [106,107].

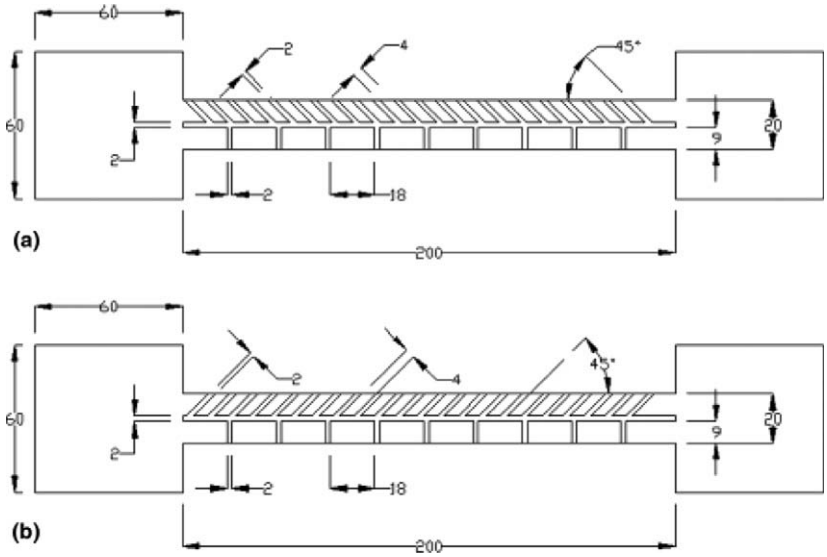

Fig. 30. Top view of designed structural geometry: (a) first and third film and (b) second film in the three-film stack. Dimensions are in μm. Reproduced with permission from [106].

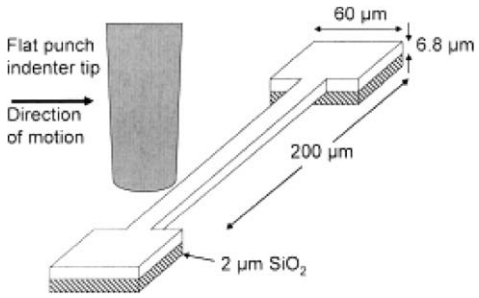

Fig. 31. Schematic illustration of a mechanical test. The load was applied in the lateral direction with a punch with a flat tip equipped with a lateral displacement transducer. Reproduced with permission from [106].

the three stacks. This could be due to the fact that the ratio of thickness of the interface (2 μm) to thickness of the lamellae (4 μm) is much larger than what is found in the structure of the conch shell. However, the bridged cracks along the ±45° interfaces in the middle layer were similar to those seen in the Queen conch shells, and the micro-composite demonstrated a significant increase in strength and work of fracture, indicating that this processing technology may be a promising method for the fabrication of artificial nacre-inspired composites, although difficult to scale to sizes of interest in engineering applications.

3.5. Self-assembly

An approach that aims to mimic not only the properties but also the processing of bioceramics is the method of self-assembly. Biomineralization involves a high degree of control over the spatial regulation of nucleation and growth of the mineral as well as the development of microarchitecture during formation. In addition, this process occurs at low-temperature in an aqueous environment from raw materials that are readily available in nature. A materials processing method that is able

to achieve such stringent control and ease of fabrication but at a faster rate than what is often found in nature is the ambitious goal of biomimetic materials processing.

The control of mineral nucleation and growth has been attempted with some success by providing a synthetic surface for nucleation. Self-assembling monolayer films and amphiphilic structures can be used to form periodic templates that influence the nucleation of ceramic phases, by varying the interface chemistry that provides a way to control the nucleation site densities. [109] However, these lacked control over the growth and ordering of the mineral phase, as well as limitations in forming multi-layered structures.

The ability to form well ordered multilayered organic/inorganic structures through self-assembly was demonstrated by Brinker and coworkers, [110] who devised an assembly process for a (PDM)/silica nanocomposite based on a simple dip-coating procedure. Starting from a homogenous solution of soluble silicates, surfactants, organic monomers and initiators in ethanol/water solvent, it makes use of evaporation-induced partitioning and cooperative assembly of silica-surfactant-monomer species into organized laminated structures. During dip-coating, preferential evaporation of ethanol progressively enriches the concentrations of monomer(s) and promotes partitioning of monomers and initiators into the surfactant micelles, and further, the cooperative assembly of the silica–surfactant–monomer micellar species into a laminated structure of organic and inorganic layers. More recently, this approach has also been used by Zhang et al. to form poly(tripropylene glycol diacrylate)/indium–tin–oxide nanocomposites, using the semiconductor indium–tin–oxide rather than silica as the inorganic phase [111].

A big drawback of these composites fabricated via self-assembly is the inability to form segmented layers. Segmented layered microstructure, as seen in the previous section, is a key feature in the microstructure of nacre. The segmentation allows extensive crack deflection and sliding of tablets without fracture of the ceramic phase, thus dramatically increasing the toughness of the material. These composites do not display the microstructural characteristics of nacre beyond the layered organic/inorganic structure, and the mechanical properties and deformation behavior of the laminated composites have not been investigated.

3.6. Computational design of bioinspired materials

Computer simulation can be effectively used as a tool to aid the development of bioinspired materials. Here we provide a review of two simulation studies that have led to insight into the relationship between structure and material properties (specifically for materials failure). The first case study is the design of a metallic nanocomposite; the second case study is the analysis of hierarchical structures composed of alpha-helical protein domains.

3.6.1. Bone-inspired metallic nanocomposite

The nanostructural motif of bone and the concept of hierarchical arrangement can be transferred to conventional metal–metal or metal–ceramic nano-composites. Such materials would be lightweight, very strong and provide high energy dissipation under deformation. A study of the applicability and transferability of the key design concepts that provide bone with its strength and toughness could for instance be achieved through computational design experiments carried out via molecular dynamics simulation. The use of molecular dynamics provides a detailed description of the atomistic deformation processes under loading at the nanoscale and may serve as a tool to enable the nanoengineering of hierarchical bioinspired materials, using a fundamental bottom-up approach.

A model nanocomposite material based on the design of bone has been studied using a Ni–Al nanostructure and an EAM alloy potential. This approach has been used to develop a composite structure that features a maximized flow stress (results shown in Fig. 32, where the nanocomposite design is shown in the left part and the resulting flow stress for various geometries is shown on the right) [112]. The Ni–Al nanostructure, in which Ni represents the harder metal, represents platelet reinforcements embedded in a soft Al matrix. Systematic large-scale molecular dynamics studies of size variations have shown the existence of a "strongest size" for the platelet size on flow strength under tensile loading [112]. The dominant contribution to plasticity switches over from interfacial

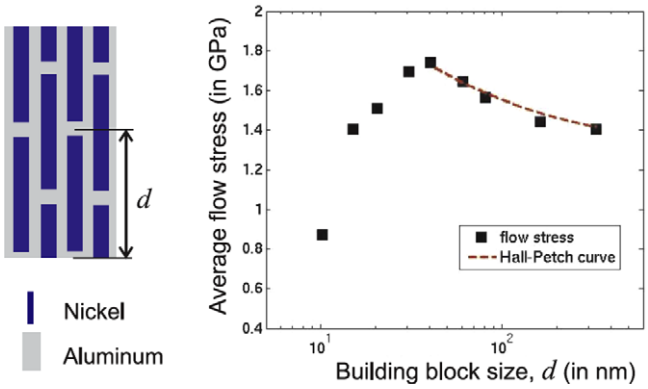

Fig. 32. Size dependence of the average flow stress (=strength) of a bioinspired metallic nanocomposite, illustrating the concept of a "strongest size" at a characteristic length-scale of material nanostructure [112]. The increase in strength scales very well according to the Hall–Petch (HP) relationship, and the reduction of strength at small building block sizes below approximately 50 nm represents an inverse Hall–Petch regime (IHP). The left part of the figure depicts the geometry of the biomicking structure of the metal nanocomposite; the results on the right display the flow stress as a function of characteristic dimension of the nanostructural arrangement.

sliding and bulk plasticity at this length-scale [112], an effect that has also been studied in single crystal analyses of metal plasticity [113].

3.6.2. Hierarchical alpha-helix based protein filaments

We review the results of another computational study, where the robustness-strength performance of alpha-helical proteins was investigated [114,115]. This study showed that with different structural arrangements, different combinations of strength and robustness can be achieved, without the use of additional material, through the combination of size-effects and hierarchical arrangement. The key questions addressed here are: (1) How can mechanically weak structural elements such as H-bonds provide the basis to strong materials? (2) What role do hierarchical structures play in providing overall mechanical properties of a material, here a protein filament? This study is of broad significance, since H-bonds are universal features of many biological materials, including spider silk, nacre (in the biopolymer phase), muscle tissue or amyloids.

We first address the question of mechanical strength of H-bonds. Fig. 33a shows the shear strength of clusters of H-bonds as a function of the size of the strand, showing a peak maximum shear strength of close to 200 MPa at a critical cluster size of 3–4 H-bonds [116]. This result illustrates that by utilizing a size effect, the fundamental limitation of H-bonds (which are mechanically weak) can be overcome. The occurrence of a strength peak at this characteristic dimension provides a possible explanation for several protein constituents, all of which display cluster of H-bonds at a similar size. Fig. 33b shows the geometry of a single alpha-helix, composed of three H-bonds per turn, corresponding to the peak of the scaling shown in Fig. 32a.

We continue now with a study of how the performance in the strength-robustness domain changes if several alpha-helices (each of which at the optimal scale for maximum strength) are assembled in different hierarchical patterns, as shown schematically in the plot (for eight alpha-helices). In this analysis, the concept of robustness is defined as flaw tolerance; it is defined as the strength of an intact filament divided by the strength of a filament in which one element is missing at the smallest level. Fig. 33c depicts results for eight subelements in the protein filament (note that the definition of subelements and their arrangement are those shown in Fig. 33b). The analysis shows that even though no additional material is used, the mechanical performance changes significantly as the hierarchical arrangement is varied. Fig. 33d depicts results for a much larger number of elements (16,384) in the protein filament [114,115]. An analysis of the distribution of structures and their performance shows that most data points (>98%) in (c) fall onto a curve referred to as the banana-curve (where

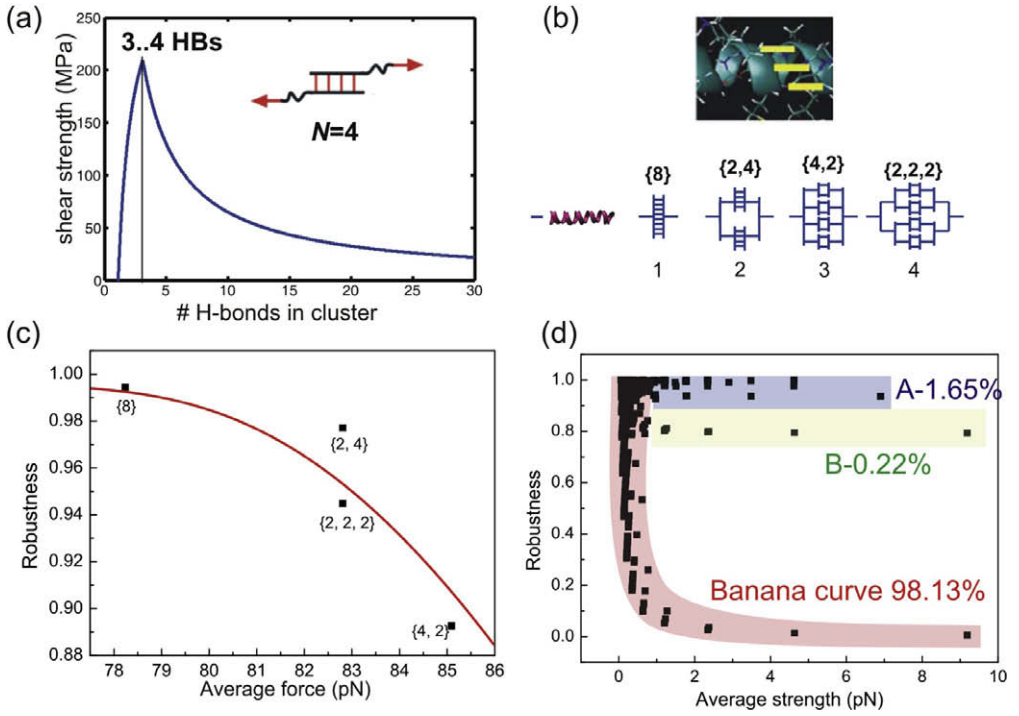

Fig. 33. Size effect and strength-robustness relation for alpha-helical protein filaments, composed out of clusters of H-bonds: (a) shows the shear strength of clusters of H-bonds as a function of the size of the strand, showing a peak maximum shear strength of close to 200 MPa at a critical cluster size of 3–4 H-bonds. By utilizing a size effect, the fundamental limitation of H-bonds of being mechanically weak can be overcome [116,119]; (b) shows the geometry of a single alpha-helix, composed of three H-bonds per turn. We study how the performance in the strength-robustness domain changes if several alpha-helices are assembled in different hierarchical patterns, as shown schematically in the plot (for eight alpha-helices); (c) depicts results for eight subelements in the protein filament. The definition of subelements and their arrangement are those shown in (b); (d) depicts results for 16,384 subelements in the protein filament [114,115]. An analysis of the distribution of structures and their performance shows that most data points (>98%) in (d) fall onto the banana-curve. Only less than 2% of all structures lead to high strength and high robustness. This analysis shows how high-performance materials can be made out of relatively weak constituents such as alpha-helices that are bonded by mechanically inferior H-bonds [114–116,118,119].

strength and robustness are exclusive properties). Only less than 2% of all structures lead to high strength and high robustness. This analysis shows how high-performance materials can be made out of relatively weak constituents such as alpha-helices that are bonded by mechanically inferior H-bonds, by arranging them into very specific hierarchical patterns.

The resulting robustness-strength plots suggest a similar behavior as that found in many biological materials (see Fig. 1b). The use of hierarchies represents an additional design variable that enables us to overcome the disparity between strength and robustness. At the same material use, hierarchical structures are capable of combing high strength and high robustness, referred to as the inverse behavior. Hierarchies may be the key to enable the type of material performance as seen in biological structures. The particular type of hierarchical structure matters. For a large number of constitutive elements (16,384) most "random" hierarchical structures fall onto the so-called banana curve on which strength and robustness remain exclusive. Only less than 2% of all structures provide the inverse behavior. This distribution of performance characteristics for a large number of elements may explain why most engineered materials show a poor performance of strength and robustness. Most randomly picked arrangements fall on the banana curve. Up until now, the hierarchical nanostructural geometries have not yet been utilized for most engineering applications (e.g., materials design). Our results show that very specific geometries are required to achieve superior performance. Biological

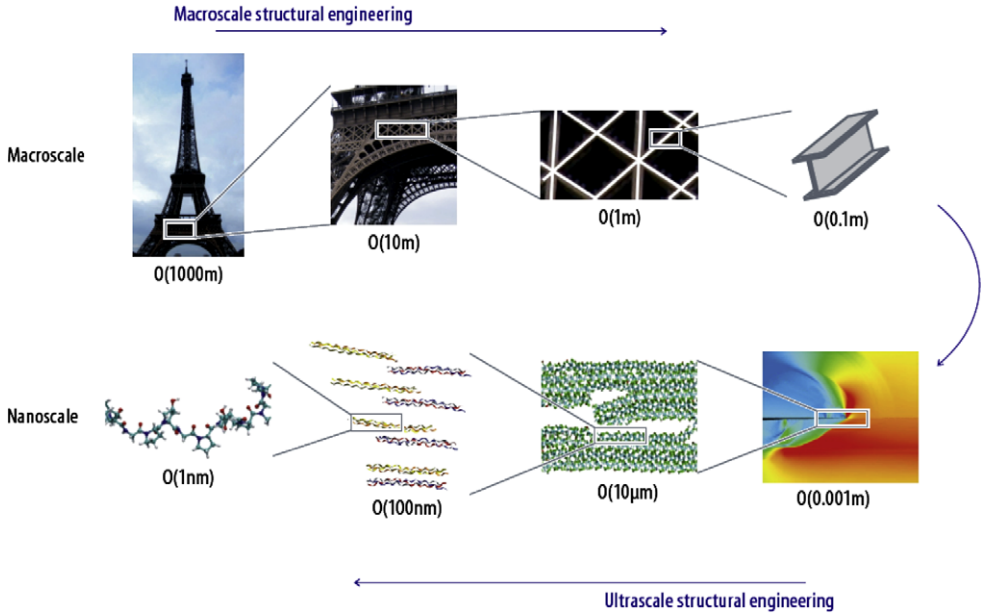

Fig. 34. Merger of structure and material in engineering design [117]. The long term impact of studying the structural makeup and properties of biological materials is that it could extend our ability to perform structural engineering at macroscale, to the ultimate scale, the nanoscale. Opening the structural material scale as design space for new material development may open great possibilities for development of robust, adaptive, active and smart materials.

materials may have achieved these particular structures through evolutionary adaptation of hierarchical structures. It suggests that biology has long implemented the efficient use of hierarchy as a materials "design" variable and established highly adapted geometries. This analysis further shows how high-performance materials can be made out of relatively weak constituents such as alpha-helices that are bonded by mechanically inferior H-bonds. Many biological materials may have developed under evolutionary pressure to yield materials with multiple objectives, such as high strength and high robustness, a trait that can be achieved by utilization of hierarchical structures. The use of these concepts may enable the development of self-assembled *de novo* bioinspired nanomaterials based on peptide and protein building blocks.

4. Conclusions and outlook

Much progress has been made in characterizing the structure and mechanical properties of mollusc shells and other biological materials such as bone. However, a number of issues remain unresolved. In particular, the specific roles of nanograins, mineral bridges and nanoasperities in nacre needs further investigation. Likewise, general constitutive laws for these materials along various loading paths are currently unavailable. Furthermore, a general acceptance within the community as to which micro/nanostructural features are essential to the material performance and which ones are less relevant needs to be achieved. The joint application of experiment and theoretical simulation approaches might play a crucial role in advancing our understanding towards that end.

An important overarching feature of biological materials is that they feature an array of size effects, observed at distinct length-scales. Such size effects may play a crucial role in overcoming the intrinsic inferiority of the building blocks of many biological materials, as shown for instance for clusters of H-bonds (see Fig. 33a). Hierarchies are used to bridge the properties of these clusters to larger length-scales, and to create biological materials that unify disparate properties (such as strength and robustness). This has been shown in Fig. 33c and d. Thus length-effects and hierarchical effects

are closely linked together, and their joint investigation must drive further analysis of all biological materials. Whereas the analysis of biological material is promising, its impact in the design of new materials remains to be seen. Some preliminary studies have been reviewed in Section 3, where the use of experimental and computational methods has been reviewed.

Over the last centuries, engineers have developed quantitative analytic and synthetic understanding of how to create complex structures out of a diverse range of constituents, at various scales (machines, buildings, airplanes, nuclear reactors and many others). Research in the area of material properties of biological materials will extend our ability to carry out structural engineering, as used for buildings or bridges today, to the ultimate scale – nanoscale, and may be a vital component of the realization of nanotechnology through the merger of material and structure [117] (Fig. 34). The merits of polymers, membranes and other nanostructures could not be utilized sufficiently unless the signal or motion at atomistic scale can be represented though macroscopic functions. Materiomics, the systematic analysis of biological materials within the materials science paradigm [118,119], may provide a new approach in engineering to create materials that have low impact on environment and energy utilization but are highly effective and functional (e.g., mechanomutable, thermomutable, controllable, changeable, etc.).

The reader will note that our review provides some perspective on the important issue of understanding these important mechanisms. Furthermore, some consensus as to what materials and performances constitute biomimicking of mollusc shells is needed. We propose two metrics: (i) materials that exhibit similar improvements in toughness when compared to their constituents; (ii) materials that exhibit similar deformation mechanisms leading to damage spreading and generation of process zones millimeters in size. In the absence of such consensus, a risk of labeling new materials as mollusc shell-liked materials, which may have been inspired by them but that do not meet suitable performance metrics, will continue to be reported in the literature. Such trend is undesirable and should be avoided to eliminate confusion and/or misunderstandings that detract from the biomimicking goals.

Advances in *in situ* microscopy experiments along with detailed multiscale modeling (as discussed in Section 1.2) have the potential to facilitate and enhance our understanding of the relationship between material microstructure and mechanical properties. Likewise, creative and innovative methods for the manufacturing of artificial shell materials are emerging. However, much work remains to be done in order to obtain morphological and chemical control at interfaces, which is required to achieve the performance exhibited by mollusc shells. One lesson from studying these materials is that the desirable inelastic deformation mechanisms are the result of complex synergies between the constituents and the hierarchy of structural features. Therefore, *successful* biomimicking of mollusc shells will require optimum selection of constituent materials and cost effective scalable manufacturing approaches capable of reproducing essential microstructural features. It is anticipated that experiments and modeling will continue to be vital in addressing this challenge.

Acknowledgements

This work was supported by the National Science Foundation through award No. CMS-0301416 and General Motors Corporation under contract No. TCS10643. HDE would like to thank Drs. Ken Chong and Pablo Zavattieri for their encouragement and support during this investigation. Special thanks are due to D. Gregoire, F. Latourte, A. Juster and O. Loh for obtaining the SEM image of nacre in the process zone and the results of nacre-like composites obtained by rapid prototyping. MJB acknowledges support from the Army Research Office (Grant # W911NF-06-1-0291), the National Science Foundation CAREER Award (Grant # 0642545), and from the Air Force Office of Scientific Research (Grant # FA9550-08-1-0321).

References

[1] Sarikaya M, Aksay IA, editors. Biomimetics design and processing of materials. Polymers and complex materials. Woodbury (NY): AIP; 1995.
[2] Mayer G. Rigid biological systems as models for synthetic composites science 2005;310(5751):1144–7.

[3] Chen P-Y, Lin AY-M, Stokes AG, Seki Y, Bodde SG, Mckittrick J, et al. Structural biological materials: overview of current research. J Met 2008;60(66):23.
[4] Verma D, Katti K, Katti D, Mohanty B. Mechanical response and multilevel structure of biomimetic hydroxyapatite/polygalacturonic/chitosan nanocomposites. Mater Sci Eng C – Biomim Supramol Syst 2008;28(3):399–405.
[5] Meyers M, Lin A, Seki Y, Chen P, Kad B, Bodde S. Structural biological composites: an overview. J Met 2006;58(7):35.
[6] Wegst UGK, Ashby MF. The mechanical efficiency of natural materials. Philos Mag 2004;84(21):2167–81.
[7] Currey JD. The design of mineralised hard tissues for their mechanical functions. J Exp Biol 1999;202(23):3285–94.
[8] Gao HJ, Ji BH, Jager IL, Arzt E, Fratzl P. Materials become insensitive to flaws at nanoscale: lessons from nature. Proc Natl Acad Sci USA 2003;100(10):5597–600.
[9] Ballarini R, Kayacan R, Ulm FJ, Belytschko T, Heuer AH. Biological structures mitigate catastrophic fracture through various strategies. Int J Fract 2005;135(1–4):187–97.
[10] Barthelat F, Li CM, Comi C, Espinosa HD. Mechanical properties of nacre constituents and their impact on mechanical performance. J Mater Res 2006;21(8):1977–86.
[11] Aizenberg J, Weaver JC, Thanawala MS, Sundar VC, Morse DE, Fratzl P. Skeleton of *Euplectella* sp.: structural hierarchy from the nanoscale to the macroscale. Science 2005;309(5732):275–8.
[12] Kohn AJ. In: Pagel M, editor. Encyclopedia of evolution: molluscs, vol. 2. Oxford University Press; 2002.
[13] Lin AYM, Chen PY, Meyers MA. The growth of nacre in the abalone shell. Acta Biomater 2008;4:31–138.
[14] Currey JD, Taylor JD. The mechanical behavior of some molluscan hard tissues. J Zool (London) 1974;173(3):395–406.
[15] Lin A, Meyers M, Vecchio K. Mechanical properties and structure of *Strombus gigas*, *Tridacna gigas*, and *Haliotis rufescens* sea shells: a comparative study. Mater Sci Eng C – Biomim Supramol Syst 2006;26(8):1380–9.
[16] Jackson AP, Vincent JFV, Turner RM. The mechanical design of nacre. Proc Roy Soc Lond 1988;234(1277):415–40.
[17] Wang RZ, Suo Z, Evans AG, Yao N, Aksay IA. Deformation mechanisms in nacre. J Mater Res 2001;16:2485–93.
[18] Kotha SP, Li Y, Guzelsu N. Micromechanical model of nacre tested in tension. J Mater Sci 2001;36(8):2001–7.
[19] Barthelat F, Tang H, Zavattieri PD, Li CM, Espinosa HD. On the mechanics of mother-of-pearl: a key feature in the material hierarchical structure. J Mech Phys Solid 2007;55(2):225–444.
[20] Smith BL, Schaffer TE, Viani M, Thompson JB, Frederick NA, Kindt J, et al. Molecular mechanistic origin of the toughness of natural adhesives fibres and composites. Nature 1999;399(6738):761–3.
[21] Prater CB, Butt HJ, Hansma PK. Atomic force microscopy. Nature 1990;345(6278):839–40.
[22] Sun YL, Luo ZP, Fertala A, An KN. Stretching type II collagen with optical tweezers. J Biomech 2004;37(11):1665–9.
[23] Dao M, Lim CT, Suresh S. Mechanics of the human red blood cell deformed by optical tweezers. J Mech Phys Solid 2003;51(11–12):2259–80.
[24] Tai K, Ulm FJ, Ortiz C. Nanogranular origins of the strength of bone. Nano Lett 2006;11:2520–5.
[25] Lim CT, Zhou EH, Li A, Vedula SRK, Fu HX. Experimental techniques for single cell and single molecule biomechanics. Mater Sci Eng C – Biomim Supramol Syst 2006;26(8):1278–88.
[26] Eppell SJ, Smith BN, Kahn H, Ballarini R. Nano measurements with micro-devices: mechanical properties of hydrated collagen fibrils. J Roy Soc Interface 2006;3(6):117–21.
[27] Zhu Y, Espinosa HD. An electromechanical material testing system for *in situ* electron microscopy and applications. Proc Natl Acad Sci USA 2005;102(41):14503–8.
[28] Espinosa HD, Zhu Y, Moldovan N. Design and operation of a MEMS-based material testing system for nanomechanical characterization. J Microelectromech Syst 2007;16(5):1219–31.
[29] Peng B, Locascio M, Zapol P, Li SY, Mielke SL, Schatz GC, et al. Measurements of near-ultimate strength for multiwalled carbon nanotubes and irradiation-induced crosslinking improvements. Nature Nanotechnol 2008;3(10):626–31.
[30] Vashishta P, Kalia RK, Nakano A. Large-scale atomistic simulations of dynamic fracture. Comput Sci Eng 1999:56–65.
[31] Rountree CL, Kalia RK, Lidorikis E, Nakano A, Brutzel LV, Vashishta P. Atomistic aspects of crack propagation in brittle materials: Multimillion atom molecular dynamics simulations. Ann Rev Mater Res 2002;32:377–400.
[32] Buehler MJ. Atomistic modeling of materials failure. New York: Springer; 2008.
[33] Tozzini V. Coarse-grained models for proteins. Curr Opin Struct Biol 2005;15(2):144–50.
[34] Tirion M. Large amplitude elastic motions in proteins from a single-parameter, atomic analysis. Phys Rev Lett 1996;77(9):1905–8.
[35] Haliloglu T, Bahar I, Erman B. Gaussian dynamics of folded proteins. Phys Rev Lett 1997;79(16):3090–3.
[36] Hayward S, Go N. Collective variable description of native protein dynamics. Ann Rev Phys Chem 1995;46:223–50.
[37] Bahar I, Jernigan R. Inter-residue potentials in globular proteins and the dominance of highly specific hydrophilic interactions at close separation. J Mol Biol 1997;266(1):195–214.
[38] Nguyen H, Hall C. Molecular dynamics simulations of spontaneous fibril formation by random-coil peptides. Proc Natl Acad Sci USA 2004;101(46):16180–5.
[39] Nguyen H, Hall C. Spontaneous fibril formation by polyalanines; discontinuous molecular dynamics simulations. J Am Chem Soc 2006;128(6):1890–901.
[40] Freddolino P, Arkhipov A, Schulten K. Coarse-grained molecular dynamics simulations of rotation-induced structural transitions in the bacterial flagellum. Biophys J 2007:142A.
[41] Buehler MJ. Nature designs tough collagen: explaining the nanostructure of collagen fibrils. Proc Natl Acad Sci USA 2006;103(33):12285–90.
[42] Buehler M. Molecular nanomechanics of nascent bone: fibrillar toughening by mineralization. Nanotechnology 2007;18(29).
[43] Barthelat F, Tang H, Zavattieri P, Li C, Espinosa HD. On the mechanics of mother-of-pearl: a key feature in the material hierarchical structure. J Mech Phys Solid 2007;55(2):306–37.
[44] Evans AG, Suo Z, Wang RZ, Aksay IA, He MY, Hutchinson JW. Model for the robust mechanical behavior of nacre. J Mater Res 2001;16(9):2475–84.
[45] Smith BL, Schaeffer TE, Viani M, Thompson JB, Frederick NA, Kindt J, et al. Molecular mechanistic origin of the toughness of natural adhesives fibres and composites. Nature (London) 1999;399(6738):761–3.
[46] Song F, Bai YL. Effects of nanostructures on the fracture strength of the interfaces in nacre. J Mater Res 2003;18:1741–4.

[47] Meyers MA, Lin AYM, Chen PY, Muyco J. Mechanical strength of abalone nacre: role of the soft organic layer. J Mech Behav Biomed Mater 2008;1(1):76–85.
[48] Su XW, Belcher AM, Zaremba CM, Morse DE, Stucky GD, Heuer AH. Structural and microstructural characterization of the growth lines and prismatic microarchitecture in red abalone shell and the microstructures of abalone "flat pearls". Chem Mater 2002;14(7):3106–17.
[49] Lin A, Meyers MA. Growth and structure in abalone shell. Mater Sci Eng A – Struct Mater Prop Microstruct Process 2005;390(1-2):27–41.
[50] Tang H, Barthelat F, Espinosa HD. An elasto-viscoplastic interface model for investigating the constitutive behavior of nacre. J Mech Phys Solid 2007;55(7):1410–38.
[51] Blank S, Arnoldi M, Khoshnavaz S, Treccani L, Kuntz M, Mann K, et al. The nacre protein perlucin nucleates growth of calcium carbonate crystals. J Microsc – Oxford 2003;212:280–91.
[52] Feng QL, Cui FZ, Pu G, Wang RZ, Li HD. Crystal orientation, toughening mechanisms and a mimic of nacre. Mater Sci Eng C – Biomim Supramol Syst 2000;11(1):19–25.
[53] Manne S, Zaremba CM, Giles R, Huggins L, Walters DA, Belcher A, et al. Atomic-force microscopy of the nacreous layer in mollusk shells. Proc Roy Soc Lond Ser B – Biol Sci 1994;256(1345):17–23.
[54] Song F, Zhang XH, Bai YL. Microstructure in a biointerface. J Mater Sci Lett 2002;21:639–41.
[55] Bruet BJF, Qi HJ, Boyce MC, Panas R, Tai K, Frick L, et al. Nanoscale morphology and indentation of individual nacre tablets from the gastropod mollusc *Trochus niloticus*. J Mater Res 2005;20(9):2400–19.
[56] Li XD, Chang WC, Chao YJ, Wang RZ, Chang M. Nanoscale structural and mechanical characterization of a natural nanocomposite material: the shell of red abalone. Nano Lett 2004;4(4):613–7.
[57] Rousseau M, Lopez E, Stempfle P, Brendle M, Franke L, Guette A, et al. Multiscale structure of sheet nacre. Biomaterials 2005;26(31):6254–62.
[58] Schaeffer TE, IonescuZanetti C, Proksch R, Fritz M, Walters DA, Almqvist N, et al. Does abalone nacre form by heteroepitaxial nucleation or by growth through mineral bridges? Chem Mater 1997;9(8):1731–40.
[59] Currey JD. Mechanical properties of mother of pearl in tension. Proc Roy Soc Lond 1977;196(1125):443–63.
[60] Barthelat F, Espinosa HD. An experimental investigation of deformation and fracture of nacre-mother of pearl. Exp Mech 2007;47(3):311–24.
[61] Menig R, Meyers MH, Meyers MA, Vecchio KS. Quasi-static and dynamic mechanical response of *Haliotis rufescens* (abalone) shells. Acta Mater 2000;48.
[62] Barthelat F, Espinosa HD. Mechanical properties of nacre constituents: an inverse method approach. In: MRS 2004 fall meeting, Boston; 2005.
[63] Katti DR, Katti KS. Modeling microarchitecture and mechanical behavior of nacre using 3D finite element techniques. Part 1. Elastic properties. J Mater Sci 2001;36:1411–7.
[64] Li XD, Xu ZH, Wang RZ. *In situ* observation of nanograin rotation and deformation in nacre. Nano Lett 2006;6(10):2301–4.
[65] Ji BH, Gao HJ. Mechanical properties of nanostructure of biological materials. J Mech Phys Solid 2004;52(9):1963–90.
[66] Zavattieri PD, Espinosa HD. Grain level analysis of crack initiation and propagation in brittle materials. Acta Mater 2001;49(20):4291–311.
[67] Espinosa HD, Zavattieri PD. A grain level model for the study of failure initiation and evolution in polycrystalline brittle materials. Part I: Theory and numerical implementation. Mech Mater 2003;35(3-6):333–64.
[68] Espinosa HD, Zavattieri PD. A grain level model for the study of failure initiation and evolution in polycrystalline brittle materials. Part II: Numerical examples. Mech Mater 2003;35(3-6):365–94.
[69] Zavattieri PD, Espinosa HD. An examination of the competition between bulk behavior and interfacial behavior of ceramics subjected to dynamic pressure-shear loading. J Mech Phys Solid 2003;51(4):607–35.
[70] Lawn BR. Fracture of brittle solids. 2nd ed. Cambridge solid state science series. New York: Cambridge University Press; 1993.
[71] Kruzic J, Nalla RK, Kinney JH, Ritchie RO. Crack bluntingM, crack bridging and resistance-curve fracture mechanics in dentin: effect of hydration. Biomaterials 2003;24(28):5209–21.
[72] Nalla RK, Kruzic JJ, Kinney JH, Ritchie RO. Mechanistic aspects of fracture and R-curve behavior in human cortical bone. Biomaterials 2005;26(2):217–31.
[73] Budiansky B, Hutchinson JW, Lambropoulos JC. Continuum theory of dilatant transformation toughening in ceramics. Int J Solid Struct 1983;19(4):337–55.
[74] Evans AG, Ahmad ZB, Gilbert DG, Beaumont PWR. Mechanisms of toughening in rubber toughened polymers. Acta Metall 1986;34(1):79–87.
[75] Du J, Thouless MD, Yee AF. Development of a process zone in rubber-modified epoxy polymers. Int J Fract 1998;92(3):271–85.
[76] Evans AG, Hutchinson JW. Effects of non-planarity on the mixed-mode fracture-resistance of bimaterial interfaces. Acta Metall 1989;37(3):909–16.
[77] Evans AG. Perspective on the development of high-toughness ceramics. J Am Ceram Soc 1990;73(2):187–206.
[78] Foulk J, Johnson G, Klein P, Ritchie R. On the toughening of brittle materials by grain bridging: promoting intergranular fracture through grain angle, strength and toughness. J Mech Phys Solid 2008;56:2381–400.
[79] Weiner S, Wagner HD. The material bone: structure mechanical function relations. Annu Rev Mater Sci 1998;28:271–98.
[80] Currey JD. Bones: structure and mechanics. Princeton (NJ): Princeton University Press; 2002.
[81] Ramachandran GN, Kartha G. Structure of collagen. Nature 1955;176:593–5.
[82] Buehler MJ. Atomistic and continuum modeling of mechanical properties of collagen: elasticity, fracture and self-assembly. J Mater Res 2006;21(8):1947–61.
[83] Buehler MJ, Wong SY. Entropic elasticity controls nanomechanics of single tropocollagen molecules. Biophys J 2007;93(1):37–43.
[84] Buehler MJ. Nanomechanics of collagen fibrils under varying cross-link densities: atomistic and continuum studies. J Mech Behav Biomed Mater 2008;1(1):59–67.

[85] Gautieri A, Buehler MJ, Redaelli A. Deformation rate controls elasticity and unfolding pathway of single tropocollagen molecules. J Mech Behav Biomed Mater 2009;2(2):130–7.
[86] Weiner S, Wagner HD. The material bone: structure–mechanical function relations. Annu Rev Mater Sci 1998;28:271–98.
[87] Nalla RK, Kinney JH, Ritchie RO. Mechanistic fracture criteria for the failure of human cortical bone. Nat Mater 2003;2(3):164–8.
[88] Fantner GE, Oroudjev E, Schitter G, Golde LS, Thurner P, Finch MM, et al. Sacrificial bonds and hidden length: unraveling molecular mesostructures in tough materials. Biophys J 2006;90(4):1411–8.
[89] Fantner GE, Hassenkam T, Kindt JH, Weaver JC, Birkedal H, Pechenik L, et al. Sacrificial bonds and hidden length dissipate energy as mineralized fibrils separate during bone fracture. Nat Mater 2005;4(8):612–6.
[90] Buehler MJ, Yung Y. Deformation and failure of protein materials in physiologically extreme conditions and disease. Nat Mater 2009:3 175–188.
[91] Alberts B, Johnson A, Lewis J, Raff M, Roberts K, Walter P. Molecular biology of the cell. Taylor & Francis; 2002.
[92] Ackbarow T, Buehler MJ. Hierarchical coexistence of universality and diversity controls robustness and multi-functionality in protein materials. Theor Comput Nanosci 2008;5(7):1193–204.
[93] Ortiz C, Boyce MC. Materials science – bioinspired structural materials. Science 2008;319(5866):1053–4.
[94] Clegg WJ, Kendall K, Alford NM, Button TW, Birchall JD. A simple way to make tough ceramics. Nature 1990;347(6292):455–7.
[95] Mayer G. New classes of tough composite materials: lessons from natural rigid biological systems. Mater Sci Eng C – Biomim Supramol Syst 2006;26(8):1261–8.
[96] Rim J, Zavattieri PD, Espinosa HD. Dimensional analysis and parametric studies for designing artificial nacre, submitted for publication.
[97] Deville S, Saiz E, Nalla RK, Tomsia AP. Freezing as a path to build complex composites. Science 2006;311(5760):515–8.
[98] Munch E, Launey ME, Alsem DH, Saiz E, Tomsia AP, Ritchie RO. Tough bio-inspired hybrid materials. Science 2008;322:1516–20.
[99] He JL, Li WZ, Li HD. Simulation of nacre with TiN/Pt multilayers and a study of their hardness. J Mater Res 1997;12.
[100] Kato T. Polymer/calcium carbonate layered thin-film composites. Adv Mater 2000;12(20):1543–6.
[101] Wei H, Ma N, Shi F, Wang Z, Zhang X. Artificial nacre by alternating preparation of layer-by-layer polymer films and $CaCO_3$ strata. Chem Mater 2007;19:1974.
[102] Tang ZY, Kotov NA, Magonov S, Ozturk B. Nanostructured artificial nacre. Nat Mater 2003;2(6):413-U8.
[103] Podsiadlo P, Kaushik AK, Arruda EM, Waas AM, Shim BS, Xu JD, et al. Ultrastrong and stiff layered polymer nanocomposites. Science 2007;318(5847):80–3.
[104] Podsiadlo P, Liu ZQ, Paterson D, Messersmith PB, Kotov NA. Fusion of seashell nacre and marine bioadhesive analogs: high-strength nanocompoisite by layer-by-layer assembly of clay and L-3,4-dihydroxyphenylaianine polymer. Adv Mater 2007;19(7):949–+.
[105] Bonderer LJ, Studart AR, Gauckler LJ. Bioinspired design and assembly of platelet reinforced polymer films. Science 2008;319(5866):1069–73.
[106] Chen L, Ballarini R, Kahn H, Heuer AH. Bioinspired micro-composite structure. J Mater Res 2007;22(1):124–31.
[107] Kamat S, Su X, Ballarini R, Heuer AH. Structural basis for the fracture toughness of the shell of the conch *Strombus gigas*. Nature 2000;405(6790):1036–40.
[108] Su XW, Zhang DM, Heuer AH. Tissue regeneration in the shell of the giant queen conch, *Strombus gigas*. Chem Mater 2004;16(4):581–93.
[109] Heuer AH, Fink DJ, Laraia VJ, Arias JL, Calvert PD, Kendall K, et al. Innovative materials processing strategies – a biomimetic approach. Science 1992;255(5048):1098–105.
[110] Sellinger A, Weiss PM, Nguyen A, Lu YF, Assink RA, Gong WL, et al. Continuous self-assembly of organic–inorganic nanocomposite coatings that mimic nacre. Nature 1998;394(6690):256–60.
[111] Zhang X, Liu C, Wu W, Wang J. Mater Lett 2006;60:2086.
[112] Broedling NC, Hartmaier A, Buehler MJ, Gao H. The strength limit in a bio-inspired metallic nanocomposite. J Mech Phys Sol 2008;56(3):1086–104.
[113] Sen D, Buehler MJ. Crystal size controlled deformation mechanism: breakdown of dislocation mediated plasticity in single nanocrystals under geometric confinement. Phys Rev B 2008;77:195439.
[114] Ackbarow T, Buehler MJ. Alpha-helical protein domains unify strength and robustness through hierarchical nanostructures. Nanotechnology 2009;20:075103.
[115] Zhao Q, Cranford S, Ackbarow T, Buehler MJ, Robustness-strength performance of hierarchical alpha-helical protein filaments. Int J Appl Mech 2009;1(1):85–112.
[116] Keten S, Buehler MJ. Geometric confinement governs the rupture strength of H-bond assemblies at a critical length scale. Nano Lett 2008;8(2):743–8.
[117] Buehler MJ, Ackbarow T. Fracture mechanics of protein materials. Mater Today 2007;10(9):46–58.
[118] Buehler MJ, Keten S. Elasticity, strength and resilience: a comparative study on mechanical signatures of α-helix, β-sheet and tropocollagen domains. Nano Res 2008;1(1):63–71.
[119] Buehler MJ, Keten S, Ackbarow T. Theoretical and computational hierarchical nanomechanics of protein materials: deformation and fracture. Progress Mater Sci 2008;53:1101–241.
[120] Ashby MF, Gibson LJ, Wegst U, Olive R. The mechanical properties of natural materials. I. Material property charts. Proc Math Phys Sci 1995;450(1938):123–40.
[121] Fratzl P, Gupta HS, Paschalis EP, Roschger P. Structure and mechanical quality of the collagen–mineral nano-composite in bone. J Mater Chem 2004;14(14):2115–23.